Structure of liquid and glassy $ZnCl_2$

Anita Zeidler,[1] Philip S. Salmon,[1] Richard A. Martin,[1] Takeshi Usuki,[1,*] Philip E. Mason,[2] Gabriel J. Cuello,[3] Shinji Kohara,[4] and Henry E. Fischer[3]

[1]*Department of Physics, University of Bath, Bath BA2 7AY, United Kingdom*

[2]*Department of Food Science, Cornell University, Stocking Hall, Ithaca, New York 14853, USA*

[3]*Institut Laue-Langevin, 6 rue Jules Horowitz, BP 156, F-38042 Grenoble Cédex 9, France*

[4]*Japan Synchrotron Radiation Research Institute, 1-1-1 Kouto, Sayo, Hyogo 679-5198, Japan*

(Received 18 March 2010; revised manuscript received 29 July 2010; published 23 September 2010)

The method of isotope substitution in neutron diffraction was used to measure the structure of liquid $ZnCl_2$ at 332(5) °C and glassy $ZnCl_2$ at 25(1) °C. The partial structure factors were obtained from the measured diffraction patterns by using the method of singular value decomposition and by using the reverse Monte Carlo procedure. The partial structure factors reproduce the diffraction patterns measured by high-energy x-ray diffraction once a correction for the resolution function of the neutron diffractometer has been made. The results show that the predominant structural motif in both phases is the corner sharing $ZnCl_4$ tetrahedron and that there is a small number of edge-sharing configurations, these being more abundant in the liquid. The tetrahedra organize on an intermediate length scale to give a first sharp diffraction peak in the measured diffraction patterns at a scattering vector $k_{\mathrm{FSDP}} \simeq 1$ Å^{-1} that is most prominent for the Zn-Zn correlations. The results support the notion that the relative fragility of tetrahedral glass forming MX_2 liquids is related to the occurrence of edge-sharing units.

DOI: 10.1103/PhysRevB.82.104208 PACS number(s): 61.20.Qg, 61.43.Fs, 61.05.F−

I. INTRODUCTION

Molten zinc chloride, $ZnCl_2$, is a material with the MX_2 stoichiometry that can be readily supercooled to form a glass.[1] The electrical conductivity and ionic diffusion coefficients are small compared to typical molten salts[1] and the temperature dependence of the liquid viscosity shows behavior that is intermediate between "strong" glass forming systems such as SiO_2 and GeO_2 and "fragile" glass forming systems such as KCl-$BiCl_3$ and $Ca_2K_3(NO_3)_7$.[2,3] The basic structural motif in the liquid at ambient pressure is the $ZnCl_4$ tetrahedron[4–9] as in the crystal[10,11] and glass.[12,13] In the liquid and glass these motifs order on an intermediate length scale as manifested by the appearance of a so-called first sharp diffraction peak (FSDP) in the measured diffraction patterns at a scattering vector $k_{\mathrm{FSDP}} \simeq 1$ Å^{-1}.[4,7,9,13,14]

Biggin and Enderby[4] used the method of isotope substitution in neutron diffraction (ND) to measure the full set of partial structure factors for the liquid at a temperature of 327 °C and found that the FSDP originates predominantly from the Zn-Zn correlations. In addition, the mean nearest-neighbor Zn-Zn distance is comparable to the nearest-neighbor Cl-Cl distance which is not expected on the basis of a rigid ion model for the interactions in which the Coulomb repulsion between divalent cations is relatively large.[15] These observations have influenced the development of a polarizable ion model (PIM) in which the ions have full formal charges and where anion polarization effects shield Coulomb repulsion between the Zn^{2+} ions.[15] This leads to a shorter nearest-neighbor Zn-Zn distance relative to a rigid ion model and to the development of an FSDP at $\simeq 1$ Å^{-1}, thus bringing $ZnCl_2$ within the class of materials whose basic properties can be understood in terms of ionic interactions.[16] Within the Bhatia-Thornton[17] formalism, the FSDP for liquid $ZnCl_2$ appears in the partial structure factors describing *both* the density and concentration fluctuations.[18,19]

The assignment of the FSDP in liquid $ZnCl_2$ to Zn-Zn correlations has, however, been questioned by Neuefeind[20] who obtained a new set of partial structure factors by combining the x-ray diffraction (XRD) data of Ref. 8 and the neutron-diffraction data of Ref. 7 and reassigned the FSDP to Zn-Cl correlations. More recently, Soper[21,22] has discussed the sensitivity of the Zn-Zn partial structure factor extracted by Biggin and Enderby[4] to the relatively small weighting of this partial structure factor in the measured diffraction patterns and to the limitations associated with measuring their data sets with a first generation neutron diffractometer. There is also some uncertainty about the water content of the samples used by Biggin and Enderby.[4,20] In addition, Raman scattering data[23] indicate that edge-sharing tetrahedra occur in the liquid phase but, unlike glass forming systems such as $GeSe_2$ (Refs. 24–27) and GeS_2 (Ref. 28), there are no obvious features in the real-space data of Biggin and Enderby,[4] such as a distinct peak in the Zn-Zn partial pair distribution function, that support the appearance of a large number of these configurations. Recent molecular-dynamics work on tetrahedral glass forming MX_2 liquids suggests that the fragility of a melt increases with the number of edge-sharing configurations, i.e., these structural units are anticipated for liquid $ZnCl_2$.[29]

We have therefore been encouraged to remeasure the full set of partial structure factors for liquid $ZnCl_2$ by using the method of isotope substitution in neutron diffraction with modern neutron-diffraction instrumentation.[30] The aim is to resolve these outstanding discrepancies and to provide data to make a detailed comparison with the measured partial structure factors for the glass, a short account of which is given elsewhere.[31] There are very few systems for which this level of information on both the liquid and glass is available from experiment, an exception being $GeSe_2$ where corner and edge-sharing tetrahedral configurations and homopolar bonds are important features of the structure.[24–27] The

neutron-diffraction results are augmented by high-energy x-ray diffraction studies of the liquid and glass.

The paper is organized as follows. The essential theory required to understand the diffraction results is described in Sec. II and includes a short account of the method of singular value decomposition (SVD) which is used to extract partial structure factors from the measured diffraction patterns.[32] The sample preparation and characterization are then outlined in Sec. III followed by the neutron and x-ray diffraction experimental methods and a description of the reverse Monte Carlo (RMC) procedure[33,34] used to model the structure. Next, in Secs. IV A and IV B the neutron-diffraction results for the liquid and glass at both the first-order difference function and partial structure factor levels are presented along with several of the results obtained from the RMC models. As shown in Sec. IV C, the partial structure factors obtained from neutron diffraction reproduce the x-ray diffraction results once a resolution function correction is applied. In Sec. V A the structures of the liquid and glass are compared using *inter alia* the bond angle distributions and ring statistics. In Sec. V B the structures of the liquid and glass are also compared within the Bhatia-Thornton[17] formalism which separates the topological from the chemical ordering. The experimental data for the melt are then compared in Sec. V C with the most recent results obtained from molecular-dynamics simulations based upon a polarizable ion model for the atomic interactions.[35,36] Finally, the conclusions are summarized in Sec. VI.

II. THEORY

A. Neutron and x-ray diffraction

In a neutron-diffraction experiment on liquid or glassy $ZnCl_2$ the scattered intensity containing structural information can be represented by the total structure factor[37]

$$F(k) = \sum_{\alpha=1}^{\mathcal{N}} \sum_{\beta=1}^{\mathcal{N}} c_\alpha c_\beta b_\alpha b_\beta [S_{\alpha\beta}(k) - 1], \tag{1}$$

where α and β denote the chemical species, $\mathcal{N}=2$ is the number of different chemical species, c_α and b_α represent the atomic fraction and coherent scattering length of chemical species α, $S_{\alpha\beta}(k)$ is a Faber-Ziman[38] partial structure factor, and k is the modulus of the scattering vector. Consider the case when four samples are investigated that are identical in every respect except for their isotopic compositions. If these samples are Zn $^{35}Cl_2$, Zn $^{\mathrm{nat}}Cl_2$, Zn $^{\mathrm{mod}}Cl_2$, and Zn $^{37}Cl_2$, where nat denotes the natural isotopic abundance of chlorine and mod denotes a modified ^{35}Cl:^{37}Cl isotope ratio, then the corresponding total structure factors are $^{35}F(k)$, $^{\mathrm{nat}}F(k)$, $^{\mathrm{mod}}F(k)$, and $^{37}F(k)$, respectively. In matrix notation

$$\begin{pmatrix} {}^{35}F(k) \\ {}^{\mathrm{nat}}F(k) \\ {}^{\mathrm{mod}}F(k) \\ {}^{37}F(k) \end{pmatrix} = \begin{pmatrix} 0.03585(6) & 0.598(2) & 0.2928(6) \\ 0.03585(6) & 0.40764(7) & 0.2418(2) \\ 0.03585(6) & 0.198(2) & 0.169(1) \\ 0.03585(6) & 0.046(2) & 0.082(2) \end{pmatrix} \times \begin{pmatrix} S_{\mathrm{ZnZn}}(k) - 1 \\ S_{\mathrm{ClCl}}(k) - 1 \\ S_{\mathrm{ZnCl}}(k) - 1 \end{pmatrix}, \tag{2}$$

where the weighting coefficients are quoted in units of barns (1 barn$=10^{-28}$ m^2) and were calculated using bound coherent scattering lengths of $b(\mathrm{Zn})=5.680(5)$, $b(^{35}\mathrm{Cl})=11.60(2)$, $b(^{\mathrm{nat}}\mathrm{Cl})=9.5770(8)$, $b(^{\mathrm{mod}}\mathrm{Cl})=6.68(4)$, and $b(^{37}\mathrm{Cl})=3.23(6)$ fm (Ref. 39) which correspond to the isotopic enrichments used in the neutron-diffraction experiments (see Sec. III A). The partial structure factor $S_{\alpha\beta}(k)$ is related to the partial pair distribution function $g_{\alpha\beta}(r)$ by the Fourier transform relation

$$g_{\alpha\beta}(r) - 1 = \frac{1}{2\pi^2 n_0 r} \int_0^\infty \mathrm{d}k k [S_{\alpha\beta}(k) - 1] \sin(kr), \tag{3}$$

where n_0 is the atomic number density and r is a distance in real space. The mean coordination number of atoms of type β, contained in a volume defined by two concentric spheres of radii r_i and r_j centered on an atom of type α, is given by

$$\bar{n}_\alpha^\beta = 4\pi n_0 c_\beta \int_{r_i}^{r_j} \mathrm{d}r r^2 g_{\alpha\beta}(r). \tag{4}$$

By using two total structure factors it is possible to eliminate one of the partial structure factors. For example, the Zn-Zn correlations may be eliminated by forming a first-order difference function such as

$$\begin{aligned} \Delta F_{\mathrm{Cl}}(k) &\equiv {}^{35}F(k) - {}^{37}F(k) \\ &= c_{\mathrm{Cl}}^2 (b_{^{35}\mathrm{Cl}}^2 - b_{^{37}\mathrm{Cl}}^2)[S_{\mathrm{ClCl}}(k) - 1] \\ &\quad + 2c_{\mathrm{Zn}} c_{\mathrm{Cl}} b_{\mathrm{Zn}} (b_{^{35}\mathrm{Cl}} - b_{^{37}\mathrm{Cl}})[S_{\mathrm{ZnCl}}(k) - 1], \end{aligned} \tag{5}$$

where the subscript indicates that $\Delta F_{\mathrm{Cl}}(k)$ contains only those correlations involving chlorine atoms. The Zn-Cl correlations may be eliminated by forming a first-order difference function such as

$$\begin{aligned} \Delta F(k) &\equiv {}^{35}F(k) - \frac{b_{^{35}\mathrm{Cl}}}{b_{^{37}\mathrm{Cl}}} {}^{37}F(k) \\ &= c_{\mathrm{Zn}}^2 b_{\mathrm{Zn}}^2 \left(1 - \frac{b_{^{35}\mathrm{Cl}}}{b_{^{37}\mathrm{Cl}}}\right)[S_{\mathrm{ZnZn}}(k) - 1] \\ &\quad + c_{\mathrm{Cl}}^2 b_{^{35}\mathrm{Cl}} (b_{^{35}\mathrm{Cl}} - b_{^{37}\mathrm{Cl}})[S_{\mathrm{ClCl}}(k) - 1]. \end{aligned} \tag{6}$$

The weighting factors for the Cl-Cl and Zn-Cl partial structure factors in Eq. (5) are 0.552(3) barn and 0.211(2) barn, respectively, while the weighting factors for the Zn-Zn and Cl-Cl partial structure factors in Eq. (6) are −0.093(2) barn and 0.432(4) barn, respectively. The real-space functions corresponding to Eqs. (5) and (6) are given by

$$\Delta G_{\mathrm{Cl}}(r) = c_{\mathrm{Cl}}^2(b_{^{35}\mathrm{Cl}}^2 - b_{^{37}\mathrm{Cl}}^2)[g_{\mathrm{ClCl}}(r) - 1] + 2c_{\mathrm{Zn}}c_{\mathrm{Cl}}b_{\mathrm{Zn}}(b_{^{35}\mathrm{Cl}} - b_{^{37}\mathrm{Cl}})[g_{\mathrm{ZnCl}}(r) - 1] \quad (7)$$

and

$$\Delta G(r) = c_{\mathrm{Zn}}^2 b_{\mathrm{Zn}}^2\left(1 - \frac{b_{^{35}\mathrm{Cl}}}{b_{^{37}\mathrm{Cl}}}\right)[g_{\mathrm{ZnZn}}(r) - 1] + c_{\mathrm{Cl}}^2 b_{^{35}\mathrm{Cl}}(b_{^{35}\mathrm{Cl}} - b_{^{37}\mathrm{Cl}})[g_{\mathrm{ClCl}}(r) - 1], \quad (8)$$

respectively.

It is also informative to decompose a total structure factor in terms of the Bhatia-Thornton[17] number-number, concentration-concentration, and number-concentration partial structure factors denoted by $S_{NN}^{\mathrm{BT}}(k)$, $S_{CC}^{\mathrm{BT}}(k)$, and $S_{NC}^{\mathrm{BT}}(k)$, respectively, where

$$F(k) = \langle b\rangle^2[S_{NN}^{\mathrm{BT}}(k) - 1] + c_{\mathrm{Zn}}c_{\mathrm{Cl}}(b_{\mathrm{Zn}} - b_{\mathrm{Cl}})^2 \times\{[S_{CC}^{\mathrm{BT}}(k)/c_{\mathrm{Zn}}c_{\mathrm{Cl}}] - 1\} + 2\langle b\rangle(b_{\mathrm{Zn}} - b_{\mathrm{Cl}})S_{NC}^{\mathrm{BT}}(k) \quad (9)$$

and $\langle b\rangle = c_{\mathrm{Zn}}b_{\mathrm{Zn}} + c_{\mathrm{Cl}}b_{\mathrm{Cl}}$ is the average coherent scattering length. Equation (2) is then rewritten as

$$\begin{pmatrix} {}^{35}F(k) \\ {}^{\mathrm{nat}}F(k) \\ {}^{\mathrm{mod}}F(k) \\ {}^{37}F(k) \end{pmatrix} = \begin{pmatrix} 0.927(3) & 0.0779(5) & -1.140(5) \\ 0.6853(3) & 0.03375(9) & -0.6452(7) \\ 0.403(3) & 0.0022(2) & -0.127(6) \\ 0.164(3) & 0.0133(7) & 0.198(3) \end{pmatrix} \times \begin{pmatrix} S_{NN}^{\mathrm{BT}}(k) - 1 \\ S_{CC}^{\mathrm{BT}}(k)/c_{\mathrm{Zn}}c_{\mathrm{Cl}} - 1 \\ S_{NC}^{\mathrm{BT}}(k) \end{pmatrix}, \quad (10)$$

where the weighting coefficients are again quoted in units of barns. The $S_{IJ}^{\mathrm{BT}}(k)$ $(I,J=N,C)$ are related to the Faber-Ziman partial structure factors $S_{\alpha\beta}(k)$ via the relations

$$S_{NN}^{\mathrm{BT}}(k) = c_{\mathrm{Zn}}^2 S_{\mathrm{ZnZn}}(k) + c_{\mathrm{Cl}}^2 S_{\mathrm{ClCl}}(k) + 2c_{\mathrm{Zn}}c_{\mathrm{Cl}}S_{\mathrm{ZnCl}}(k), \quad (11)$$

$$S_{CC}^{\mathrm{BT}}(k) = c_{\mathrm{Zn}}c_{\mathrm{Cl}}\{1 + c_{\mathrm{Zn}}c_{\mathrm{Cl}}[S_{\mathrm{ZnZn}}(k) + S_{\mathrm{ClCl}}(k) - 2S_{\mathrm{ZnCl}}(k)]\}, \quad (12)$$

$$S_{NC}^{\mathrm{BT}}(k) = c_{\mathrm{Zn}}c_{\mathrm{Cl}}\{c_{\mathrm{Zn}}[S_{\mathrm{ZnZn}}(k) - S_{\mathrm{ZnCl}}(k)] - c_{\mathrm{Cl}}[S_{\mathrm{ClCl}}(k) - S_{\mathrm{ZnCl}}(k)]\}. \quad (13)$$

As shown by Eq. (9), $S_{NN}^{\mathrm{BT}}(k)$ would be measured directly in a diffraction experiment on $ZnCl_2$ if the ratio of the chlorine isotopes was chosen such that $b_{\mathrm{Cl}} = b_{\mathrm{Zn}}$. The Fourier transform of this function, $g_{NN}^{\mathrm{BT}}(r)$, therefore describes the sites of the scattering nuclei but does not distinguish between the chemical species that occupy those sites, i.e., it gives information on the topological ordering. By comparison, $S_{CC}^{\mathrm{BT}}(k)$ would be measured directly in a diffraction experiment if $\langle b\rangle = 0$ and its Fourier transform, $g_{CC}^{\mathrm{BT}}(r)$, gives information on the decoration by Zn and Cl of the sites described by $g_{NN}^{\mathrm{BT}}(r)$. A preference for like or unlike neighbors at a given distance will lead to a corresponding positive or negative peak in $g_{CC}^{\mathrm{BT}}(r)$, respectively. The Fourier transform of $S_{NC}^{\mathrm{BT}}(k)$ describes the correlation between sites and their occupancy by a given chemical species. A fuller description of MX_2 systems within the Bhatia-Thornton formalism is given elsewhere.[18,19]

In an x-ray diffraction experiment, the scattered intensity containing structural information can also be represented by Eq. (1) after the neutron scattering lengths b_α are replaced by the k-dependent atomic form factors $f_\alpha(k)$. In order to compensate for this k dependence, the x-ray total structure factor is often written as

$$S_{\mathrm{X}}(k) = \frac{F_{\mathrm{X}}(k)}{|\langle f(k)\rangle|^2} + 1, \quad (14)$$

where $F_{\mathrm{X}}(k) = \sum_{\alpha=1}^{\mathcal{N}}\sum_{\beta=1}^{\mathcal{N}} c_\alpha c_\beta f_\alpha(k) f_\beta^*(k)[S_{\alpha\beta}(k) - 1]$ and $\langle f(k)\rangle = c_{\mathrm{Zn}}f_{\mathrm{Zn}}(k) + c_{\mathrm{Cl}}f_{\mathrm{Cl}}(k)$.

B. Method of singular value decomposition

Equations (2) and (10) for the Faber-Ziman and Bhatia-Thornton partial structure factors can each be rewritten in the form

$$\mathbf{F} = \mathbf{WS}, \quad (15)$$

where $\mathbf{F}$ is a column vector for the total structure factors, $\mathbf{S}$ is a column vector for the partial structure factors, and $\mathbf{W}$ is an $m \times n$ weighting factor matrix (m rows and n columns) with $m > n$ and rank equal to n. The solution to this equation can be found by using SVD (Refs. 32 and 40–44) to solve the least-squares problem in which a unique $\mathbf{S}$ is found which minimizes the two-norm (or Euclidean norm), $\|\mathbf{r}\|_2$, of the residual vector $\mathbf{r} = \mathbf{F} - \mathbf{WS}$.[40,44] In the compact (or condensed) SVD representation the weighting factor matrix is written as $\mathbf{W} = \mathbf{U\Sigma V}^T$, where $\mathbf{U}$ is an $m \times n$ column orthogonal matrix, $\mathbf{\Sigma}$ is an $n \times n$ diagonal matrix with main diagonal elements $\sigma_1 \geq \sigma_2 \geq \cdots \geq \sigma_n > 0$ known as the singular values, and $\mathbf{V}^T$ is the transpose of an $n \times n$ orthogonal matrix $\mathbf{V}$.[42,44] The least-squares solution to Eq. (15) is then given by

$$\mathbf{S} = \mathbf{W}^\dagger\mathbf{F} = \sum_{l=1}^{n}\frac{(\mathbf{U}_l \cdot \mathbf{F})}{\sigma_l}\mathbf{V}_l, \quad (16)$$

where $\mathbf{W}^\dagger = \mathbf{V}[\mathrm{diag}(1/\sigma_l)]\mathbf{U}^T$ is the Moore-Penrose pseudoinverse of $\mathbf{W}$, $[\mathrm{diag}(1/\sigma_l)]$ is an $n \times n$ diagonal matrix with main diagonal elements $1/\sigma_l$, the vectors $\mathbf{U}_l$ and $\mathbf{V}_l$ denote the columns of matrices $\mathbf{U}$ and $\mathbf{V}$, respectively, and the dot product $\mathbf{U}_l \cdot \mathbf{F} = \mathbf{U}_l^T\mathbf{F}$. Thus $\mathbf{S}$ is a linear combination of the columns of $\mathbf{V}$ where the lth column $\mathbf{V}_l$ is weighted by the scalar $(\mathbf{U}_l \cdot \mathbf{F})/\sigma_l$. If $\mathbf{F}$ is subjected to an uncertainty (or error) $\delta\mathbf{F}$ then the corresponding uncertainty $\delta\mathbf{S}$ on $\mathbf{S}$ is given by[44]

$$\delta\mathbf{S} = \sum_{l=1}^{n}\frac{(\mathbf{U}_l \cdot \delta\mathbf{F})}{\sigma_l}\mathbf{V}_l. \quad (17)$$

In the case of the Faber-Ziman weighting factor matrix of Eq. (2), the singular values are $\sigma_1 = 0.861$, $\sigma_2 = 0.087$, and $\sigma_3 = 0.01$ which indicates that $\mathbf{S}$ will be most sensitive to the uncertainty associated with the $l=3$ term. Successive compo-

nents in the column vector $\mathbf{V}_3=[0.911,0.141,-0.388]^T$ correspond to the Zn-Zn, Cl-Cl, and Zn-Cl partial structure factors, respectively. Thus an uncertainty $\delta\mathbf{F}$ will lead to errors in the Zn-Zn and Cl-Cl partial structure factors that have an opposite sign to an error in the Zn-Cl partial structure factor. In addition, the Zn-Zn partial structure factor will be the most sensitive to $\delta\mathbf{F}$ while the Cl-Cl partial structure factor will be the least sensitive. Similarly, in the case of the Bhatia-Thornton weighting factor matrix of Eq. (10), the singular values are $\sigma_1=1.781$, $\sigma_2=0.349$, and $\sigma_3=0.025$ and successive components in the column vector $\mathbf{V}_3=[0.026,-0.999,-0.039]^T$ correspond to the *N-N*, *C-C*, and *N-C* partial structure factors, respectively. Thus an uncertainty $\delta\mathbf{F}$ will lead to an error in the *N-N* partial structure factor that has an opposite sign to errors in the *C-C* and *N-C* partial structure factors. Also, the *C-C* partial structure factor will be the most sensitive to $\delta\mathbf{F}$ while the *N-N* partial structure factor will be the least sensitive.

The two-norm condition number of the weighting factor matrix (sometimes called a Turing number[32]) is given by $\kappa_2=\sigma_1/\sigma_n$, where σ_1 and σ_n are the largest and smallest singular values of $\mathbf{W}$, respectively.[43,44] Thus $\kappa_2\geq 1$ and values near unity indicate a well conditioned matrix.[41,44] Let $\delta\mathbf{W}$ be the uncertainty on $\mathbf{W}$ such that $\|\delta\mathbf{W}\|_2/\|\mathbf{W}\|_2<1/\kappa_2$ (which can be rewritten as $\|\delta\mathbf{W}\|_2\|\mathbf{W}^\dagger\|_2<1$) where $\|\mathbf{A}\|_2$ denotes the two-norm (or spectral norm) of matrix $\mathbf{A}$, which can be calculated by finding the square root of the largest eigenvalue of $\mathbf{A}^T\mathbf{A}$ and is equal to the largest singular value of $\mathbf{A}$. Then an upper bound on the relative uncertainty in $\mathbf{S}$ is provided by the expression[40]

$$\frac{\|\delta\mathbf{S}\|_2}{\|\mathbf{S}\|_2}\leq\frac{\kappa_2}{1-\kappa_2\|\delta\mathbf{W}\|_2/\|\mathbf{W}\|_2}\times\left[\left(1+\frac{\kappa_2\|\mathbf{r}\|_2}{\|\mathbf{W}\|_2\|\mathbf{S}\|_2}\right)\frac{\|\delta\mathbf{W}\|_2}{\|\mathbf{W}\|_2}+\frac{\|\delta\mathbf{F}\|_2}{\|\mathbf{W}\|_2\|\mathbf{S}\|_2}\right]. \tag{18}$$

This equation can also be rewritten using the relation $\|\mathbf{WS}\|_2\leq\|\mathbf{W}\|_2\|\mathbf{S}\|_2$ and, for the case when $\|\delta\mathbf{W}\|_2/\|\mathbf{W}\|_2\ll 1/\kappa_2$, the first term on the right-hand side reduces to κ_2. The presence of the $\kappa_2^2\|\mathbf{r}\|_2\|\delta\mathbf{W}\|_2/\|\mathbf{W}\|_2$ term in Eq. (18) means that a small uncertainty in $\mathbf{W}$ can have a large effect on the relative uncertainty in $\mathbf{S}$ unless the residual is sufficiently small.[44] If $\mathbf{W}$ is known exactly then Eq. (18) reduces to the expression $\|\delta\mathbf{S}\|_2/\|\mathbf{S}\|_2\leq\kappa_2\|\delta\mathbf{F}\|_2/\|\mathbf{W}\|_2\|\mathbf{S}\|_2$. It is useful to note that for an isotopic substitution experiment on a binary system in which three different total structure factors are measured to give a nonsingular $n\times n$ matrix $\mathbf{W}$ of rank equal to n, Eqs. (15)–(17) also hold except that $\mathbf{U}$ becomes an orthogonal $n\times n$ matrix and $\mathbf{W}^\dagger$ is equal to the inverse matrix $\mathbf{W}^{-1}$. In this case, if $\|\delta\mathbf{W}\|_2/\|\mathbf{W}\|_2<1/\kappa_2$ then an upper bound on the relative uncertainty in $\mathbf{S}$ is given by $\|\delta\mathbf{S}\|_2/\|\mathbf{S}\|_2\leq[\kappa_2/(1-\kappa_2\|\delta\mathbf{W}\|_2/\|\mathbf{W}\|_2)](\|\delta\mathbf{W}\|_2/\|\mathbf{W}\|_2+\|\delta\mathbf{F}\|_2/\|\mathbf{W}\|_2\|\mathbf{S}\|_2)$.[40]

For the Faber-Ziman and Bhatia-Thornton weighting factor matrices given by Eqs. (2) and (10), κ_2 takes values of 84 and 71, respectively, i.e., the matrix for the latter is better conditioned. For these matrices, the ratio $\|\delta\mathbf{W}\|_2/\|\mathbf{W}\|_2$ takes values of 0.005 and 0.006, respectively. The rows of Eq. (15) can, however, be multiplied by arbitrary constants thus changing the two-norm condition number of the matrix. For this reason, the two-norm condition number κ_2' for the normalized matrix $\mathbf{W}'$ is sometimes quoted[32] where the ith row of matrix $\mathbf{W}$ is divided by $(\Sigma_{j=1}^n W_{ij}^2)^{1/2}$ such that the matrix element $W_{ij}'=W_{ij}/(\Sigma_{j=1}^n W_{ij}^2)^{1/2}$. The condition numbers thus obtained for the normalized Faber-Ziman and Bhatia-Thornton matrices are $\kappa_2'=46$ and $\kappa_2'=33$, respectively. Another measure of the conditioning, often used in neutron-diffraction experiments,[45] is provided by the determinant of the normalized matrix, $|\mathbf{W}'|$, which takes values of 0.0014 and −0.004 for the Faber-Ziman and Bhatia-Thornton matrices, respectively. A well conditioned matrix corresponds to a value for $|\mathbf{W}'|$ that is close to ± 1.[46]

In view of the large potential for error, Edwards *et al.*[45] developed a method for extracting the partial structure factors from the measured data sets by imposing constraints to eliminate unphysical solutions. RMC (Refs. 33 and 34) and empirical potential structure refinement (EPSR) (Ref. 22) methods have also been developed to construct three-dimensional models that are consistent with the measured data sets. In the following, the SVD method is applied to high precision data sets for which the parameters in the data correction procedure are refined to ensure that the partial structure factors, and corresponding partial pair distribution functions, satisfy the physical constraints described in Sec. III B. The results are then compared to those obtained by using the RMC method.

III. EXPERIMENTAL AND MODELING PROCEDURES

A. Synthesis of $ZnCl_2$

Samples of HCl with isotopically enriched chlorine were prepared by the action of H_2SO_4 on isotopically enriched samples of CsCl in a high-vacuum apparatus. The HCl was then reacted with an aqueous solution of $AgNO_3$ (99.995%) to precipitate AgCl, which was washed in water and dried. Zinc metal (99.999%, 0.45 mol equivalent) was distilled under high vacuum into a sealed silica apparatus that contained the AgCl (1 mol equivalent). After 24 h at 700 °C the zinc had completely reacted with the AgCl and the resultant $ZnCl_2$ vapor (which will contain predominantly linear $ZnCl_2$ monomers with a small fraction of Zn_2Cl_4 dimers having D_{2h} symmetry where the Zn atoms are bridged by two Cl atoms[47–50]) was condensed in a cylindrical silica ampoule of 4 mm inner diameter and 1 mm wall thickness. The ampoule containing liquid $ZnCl_2$ was quenched from 400 °C in water at room temperature to give a clear colorless glass. The ampoule was then sealed under high vacuum ready for use in the diffraction experiments. An AgCl impurity content of <0.1 mol % was estimated by chemical analysis and energy dispersive neutron-scattering experiments showed no sign of the strong ^{109}Ag absorption resonance at 5.19(1) eV.[51] A neutron-diffraction experiment on a crystallized sample revealed the anhydrous (delta) phase.[10,11] The samples used for the diffraction experiments are denoted by Zn $^{35}Cl_2$, Zn $^{nat}Cl_2$, Zn $^{mod}Cl_2$, and Zn $^{37}Cl_2$ which correspond to

^{35}Cl:^{37}Cl ratios of 0.994:0.006, 0.7577:0.2423, 0.42:0.58, and 0.018:0.982, respectively.

In the case of the x-ray diffraction experiment, anhydrous beads of $ZnCl_2$ (99.999%, Sigma-Aldrich) were first sealed under a vacuum of $\approx 10^{-5}$ torr in a silica container connected to a cylindrical silica capillary tube of 1.8 mm inner diameter and 0.6 mm wall thickness. The apparatus was then placed in an oven at 800 °C with the tip of the capillary tube placed outside of the oven door. The $ZnCl_2$ vapor that was generated condensed into the cooler part of capillary tube which was subsequently sealed under high vacuum. The sample was vitrified by first heating it in the sealed capillary to ≈450 °C and then quenching in an iced water mixture.

B. Neutron-diffraction experiments

The neutron-diffraction experiments were made using the D4C instrument at the Institut Laue-Langevin (ILL) with an incident neutron wavelength of 0.49971(1) Å (glass) or 0.50040(1) Å (liquid).[30] The first diffraction experiment was made on the as-prepared glassy $ZnCl_2$ samples at 25(1) °C. Diffraction patterns were taken for each of the samples in their silica container, an empty container, the empty instrument, and a cylindrical vanadium rod of diameter 6.37(1) mm for normalization purposes. The intensity for a bar of neutron absorbing $^{10}B_4C$ of dimensions comparable to the sample was also measured to account for the effect of the sample's attenuation on the background signal at small scattering angles.[52] The same samples in the same silica ampoules were also used for the second diffraction experiment on the liquid phase of $ZnCl_2$ at 332(5) °C. For this experiment a vanadium furnace was used with a heating element of ≈17 mm diameter and 0.1 mm wall thickness together with a heat shield of 25 mm diameter and 0.04 mm wall thickness. Diffraction patterns were taken at 332(5) °C for the samples in their container in the furnace, for an empty container in the furnace, and for the empty furnace. Diffraction patterns were also taken at room temperature for the empty furnace, for a cylindrical vanadium rod of diameter 6.37(1) mm in the furnace, and for a bar of neutron absorbing $^{10}B_4C$ of dimensions comparable to the sample in the furnace.

Each complete diffraction pattern was built up from the intensities measured for the different detector groups. These intensities were saved at regular intervals and no deviations between them were observed within the counting statistics which verified the stability of both the samples and the diffractometer.[30,53] The data were carefully corrected to yield the total structure factor for each sample and the usual self-consistency checks were performed.[26,54,55] For example, it is necessary that (i) the measured intensities are greater than or equal to zero such that $S_{NN}^{BT}(k)S_{CC}^{BT}(k) \geq S_{NC}^{BT}(k)^2$ at all k values,[17] (ii) the Faber-Ziman partial structure factors satisfy the sum rule relation $\int_0^\infty [S_{\alpha\beta}(k)-1]k^2dk=-2\pi^2 n_0$ which is obtained by considering the small r limit of Eq. (3),[45] (iii) the partial pair distribution functions $g_{\alpha\beta}(r)$ oscillate about zero at r values smaller than the distance of closest approach between the center of two atoms, and (iv) when these small r oscillations are set to zero, the Fourier back transform should be in good overall agreement with the original reciprocal space data set.[55] The atomic number density of $ZnCl_2$ is 0.0359(1) $Å^{-3}$ for the glass and 0.0335(1) $Å^{-3}$ for the liquid at 332 °C.[1]

C. X-ray diffraction experiments

High-energy x-ray diffraction experiments on glassy $ZnCl_2$ at room temperature and on liquid $ZnCl_2$ at 328(1) °C were made using beamline BL04B2 at SPring-8 with an incident x-ray wavelength of 0.20095(5) Å (energy ≈61.7 keV) corresponding to the (220) planes of a silicon monochromator.[56] The incident intensity of x-rays was monitored by an ionization chamber filled with Ar gas of 99.99% purity, the samples were held in a vacuum bell jar to avoid air scattering, and the diffracted x-rays were collected using a Ge solid state detector. In the case of the glass, diffraction patterns were taken at room temperature for the sample in its container and for an empty container. In the case of the liquid, diffraction patterns were taken for the sample in its container in the furnace and for an empty container in the furnace. The x-ray data analysis procedure followed the method described elsewhere.[56] In this procedure, the ionic form factors for Zn^{2+} and Cl^- were used[57] and the Compton scattering corrections were taken from Refs. 58 and 59.

D. RMC modeling

The total structure factors measured in the neutron-diffraction experiments were used to generate RMC models for the liquid and glass using the program RMCA.[34] The models used 3000 atoms (1000 Zn and 2000 Cl) in a cubic box with a side length of 44.74 Å (liquid) or 43.72 Å (glass) chosen to give the same atomic number density as used in the neutron-diffraction data analysis procedure. Atomic configurations were generated by first taking a random configuration of particles and running a conventional hard sphere Monte Carlo (HSMC) simulation with nearest-neighbor cut-off distances of 2.0, 3.0, and 3.0 Å in the liquid and 2.0, 3.3, and 3.2 Å in the glass for the Zn-Cl, Zn-Zn, and Cl-Cl nearest-neighbor distances, respectively, i.e., particle movements are rejected if they result in nearest-neighbor distances that are smaller than these values. These values for the cut-off distances were chosen by reference to the Fourier transforms of the measured total structure factors and difference functions, e.g., in the liquid there is no evidence of Zn-Cl correlations below 2.0 Å and no evidence of Zn-Zn or Cl-Cl correlations below 3.0 Å (see Secs. IV A and IV B). Separate evidence in support of a 3.0 Å low r cut-off value for the like atom correlations comes from high-energy x-ray diffraction work on the liquid which shows a decrease in this cut-off value with increasing temperature.[60] The measured total structure factors were then used to generate RMC models, without the application of coordination number constraints, and the final results were obtained by averaging over ten independent configurations. An RMC model for the liquid was also generated using no cut-off constraints and led to nearest-neighbor cut-off distances of 2.9 Å and 3.0 Å for the Zn-Zn and Cl-Cl correlations, respectively. Previous

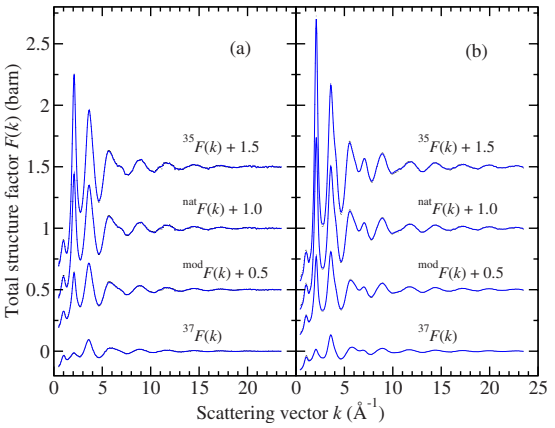

FIG. 1. (Color online) The total structure factors $F(k)$ measured by using neutron diffraction for (a) liquid $ZnCl_2$ at 332(5) °C and (b) glassy $ZnCl_2$ at 25(1) °C. The vertical bars represent the measured data points with statistical errors and the solid (blue) curves correspond to the RMC model. The discrepancy between the measured data points and the model are smaller than the line thickness at most k values.

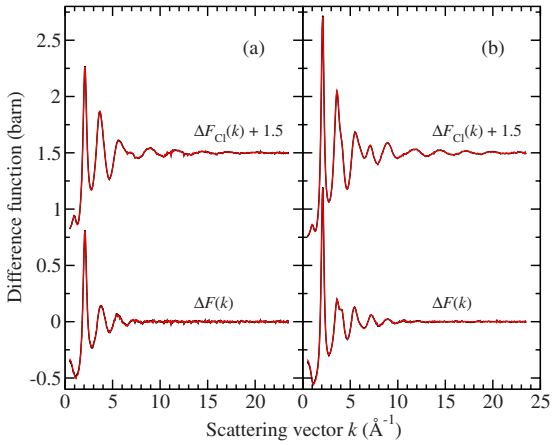

FIG. 2. (Color online) The difference functions $\Delta F_{Cl}(k)$ and $\Delta F(k)$ measured by using neutron diffraction for (a) liquid $ZnCl_2$ at 332(5) °C and (b) glassy $ZnCl_2$ at 25(1) °C. The vertical bars represent the measured data points with statistical errors and the solid (red) curves are the Fourier back transforms of the corresponding real-space difference functions $\Delta G_{Cl}(r)$ and $\Delta G(r)$ given by the solid (black) curves in Fig. 3 where the unphysical oscillations at r values smaller than the distance of closest approach between the centers of two atoms are set to the calculated $\Delta G_{Cl}(r=0)$ or $\Delta G(r=0)$ limit. For all of the functions the Fourier back transforms are indistinguishable from the data points at most k values.

RMC models of liquid and glassy $ZnCl_2$ based on older data sets are described in Refs. 9 and 61–63.

IV. RESULTS

A. Liquid $ZnCl_2$ at 332(5) °C

The total structure factors measured for the different isotopically enriched liquid samples show a large contrast and feature an FSDP at 1.01(2) Å^{-1} [see Fig. 1(a)]. As shown in Fig. 2(a), the FSDP appears as a positive feature in the difference function $\Delta F_{Cl}(k)$, where the Cl-Cl and Zn-Cl partial structure factors both have positive weighting factors [see Eq. (5)], and as a negative feature in the difference function $\Delta F(k)$, where the Zn-Zn and Cl-Cl partial structure factors have negative and positive weighting factors, respectively [see Eq. (6)]. The observations are therefore consistent with a contribution to the FSDP from both Zn-Zn and Zn-Cl correlations. The real-space difference functions $\Delta G_{Cl}(r)$ and $\Delta G(r)$ are shown in Fig. 3(a). The first peak in $\Delta G_{Cl}(r)$ at 2.27(2) Å is assigned to nearest-neighbor Zn-Cl correlations by comparison with the crystal structures of $ZnCl_2$ (Refs. 10, 11, and 64–66) and integration over this peak to the first minimum at 2.76(2) Å gives a coordination number $\bar{n}_{Zn}^{Cl}=4.1(1)$. The small r cutoff in $\Delta G_{Cl}(r)$, a function that comprises only those correlations involving Cl atoms, is at 2.02 Å and the small r cutoff in $\Delta G(r)$, a function that comprises positively weighted Cl-Cl correlations and negatively weighted Zn-Zn correlations, is at 3.01 Å.

The partial structure factors $S_{\alpha\beta}(k)$ of Fig. 4 were obtained from the measured total structure factors of Fig. 1(a) by using Eq. (16). The Zn-Zn partial structure factor has the largest error bars as expected from the discussion of Sec. II B. The results show that the largest FSDP appears in $S_{ZnZn}(k)$ and that there is also a notable feature at $\simeq 1$ Å^{-1} in $S_{ZnCl}(k)$. The partial pair distribution functions $g_{\alpha\beta}(r)$ in Fig. 5 were generated by spline fitting the $S_{\alpha\beta}(k)$ functions and Fourier transforming. The first peak in $g_{ZnCl}(r)$ at $r_{ZnCl}=2.27(2)$ Å gives a coordination number $\bar{n}_{Zn}^{Cl}=4.2(1)$, consistent with the results obtained from the difference function $\Delta G_{Cl}(r)$. The first peak in $g_{ClCl}(r)$ at $r_{ClCl}=3.68(3)$ Å gives a ratio $r_{ClCl}/r_{ZnCl}=1.62(2)$ which compares with the value of $\sqrt{8/3}=1.633$ expected for a regular $ZnCl_4$ tetrahedron. The nearest-neighbor Zn-Cl and Cl-Cl peak positions give a Cl-Zn-Cl bond angle of 108(3)° which compares with the ideal tetrahedral angle of 109.47°.

The Zn-Zn partial pair correlation function has two overlapping peaks at 2.97(3) and 3.96(3) Å and integration of

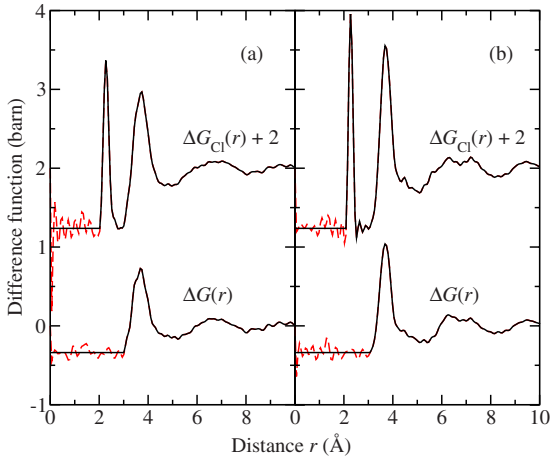

FIG. 3. (Color online) The difference functions $\Delta G_{Cl}(r)$ and $\Delta G(r)$ for (a) liquid $ZnCl_2$ at 332(5) °C and (b) glassy $ZnCl_2$ at 25(1) °C as obtained by Fourier transforming the corresponding $\Delta F_{Cl}(k)$ or $\Delta F(k)$ functions given by the points with error bars in Fig. 2. The broken (red) curves show the extent of the unphysical small r oscillations.

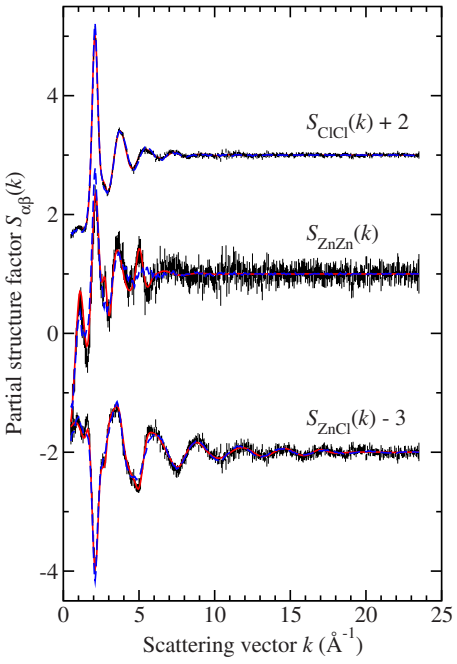

FIG. 4. (Color online) The Faber-Ziman partial structure factors $S_{\alpha\beta}(k)$ for liquid $ZnCl_2$ at 332(5) °C. The vertical bars represent the measured data points with statistical errors and were obtained from the measured total structure factors given in Fig. 1(a) by using Eq. (16). The solid (red) curves are the Fourier back transforms of the corresponding partial pair distribution functions $g_{\alpha\beta}(r)$ given by the solid (black) curves in Fig. 5 where the unphysical oscillations at r values smaller than the distance of closest approach between the centers of two atoms are set to the calculated $g_{\alpha\beta}(r=0)=0$ limit. The broken (blue) curves were obtained from the RMC model and correspond to the total structure factors given by the solid (blue) curves in Fig. 1(a).

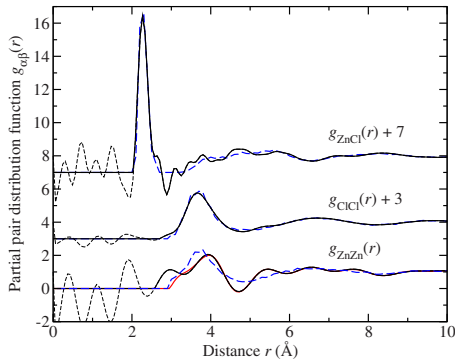

FIG. 5. (Color online) The partial pair distribution functions $g_{\alpha\beta}(r)$ for liquid $ZnCl_2$ at 332(5) °C. The solid (black) curves were obtained by Fourier transforming the measured partial structure factors $S_{\alpha\beta}(k)$ given in Fig. 4 after spline fitting and the thin broken (black) curves at small r show the extent of the unphysical oscillations at r values smaller than the distance of closest approach between the centers of two atoms. The light solid (red) curve gives the $g_{ZnZn}(r)$ function generated by a procedure that removed the first peak at 2.97(3) Å (see the text). The broken (blue) curves are from the RMC model and correspond to the broken (blue) curves in Fig. 4.

these peaks over the range 2.58–4.54 gives a coordination number $\bar{n}_{Zn}^{Zn}=4.5(2)$, somewhat larger than the value of 4 expected for a network of corner sharing $ZnCl_4$ tetrahedra. The maximum distance between the centers of two regular corner sharing tetrahedra is $2r_{ZnCl}$ which occurs when the centers and the shared corner sit on a common straight line. The calculated distance for the liquid is 4.54(4) Å which coincides with the upper limit of the second peak in $g_{ZnZn}(r)$. The crystal structures reported for $ZnCl_2$, several of which correspond to material contaminated with water, are based on corner sharing $ZnCl_4$ tetrahedra in which the Zn-Zn distance is within the range 3.70–4.06 Å.[10,11,64–66] The peak in $g_{ZnZn}(r)$ at 3.96(3) Å is therefore likely to result from corner sharing tetrahedral configurations although the value is somewhat larger than that found for the anhydrous (delta) phase of $ZnCl_2$ where $r_{ZnZn}=3.75–3.77$ Å.[10,11] In the case of regular edge-sharing tetrahedra, the maximum distance occurs when two centers and a shared edge are in the same plane. This corresponds to a distance $r_{ZnZn}=2\cos(\gamma/2)r_{ZnCl}$, where γ is the tetrahedral angle of 109.47°. The calculated distance $r_{ZnZn}=2.62(2)$ Å is comparable to the small r limit in $g_{ZnZn}(r)$ of 2.58 Å while a recalculation, using the measured Zn-Cl-Zn angle of 108(3)°, gives $r_{ZnZn}=2.67(2)$ Å. The structural origin of the peak in $g_{ZnZn}(r)$ at 2.97(3) Å is therefore puzzling, especially as the peak position is comparable to the low r cut-off value of 3.01 Å found for $\Delta G(r)$ [see Fig. 3(a)]. The peak also corresponds to a trough in $g_{ZnCl}(r)$ and, as discussed in Sec. II B, an error in the measured total structure factors is likely to lead to an error in $g_{ZnZn}(r)$ that has an opposite sign to an error in $g_{ZnCl}(r)$. To investigate further, the feature at 2.97(3) Å was removed by a procedure in which a peak in the Fourier transform of the unsmoothed Zn-Zn partial structure factor was removed, the data were Fourier back transformed into reciprocal space, and the resultant $S_{ZnZn}(k)$ function was used to generate a revised $g_{ZnZn}(r)$ function after spline fitting.[67] As shown in Fig. 5 this procedure leads to a revised low r cut-off value of 2.95(2) Å and a shoulder now appears on the small r side of the first peak in $g_{ZnZn}(r)$ at 3.96(3) Å. Integration of the first peak of the revised $g_{ZnZn}(r)$ function over the range 2.95–4.54 Å gives $\bar{n}_{Zn}^{Zn}=3.8(2)$.

The total structure factors $F(k)$, partial structure factors $S_{\alpha\beta}(k)$, and partial pair distribution functions $g_{\alpha\beta}(r)$ obtained from the RMC model for the liquid are shown in Figs. 1(a), 4, and 5, respectively. The Zn-Cl and Cl-Cl pair correlation functions are in good agreement with the measured functions obtained by using SVD but there are several discrepancies with respect to the Zn-Zn pair correlation functions. The most significant of these manifests itself in $g_{ZnZn}(r)$ where there is a single peak at 3.74(5) Å with a shoulder on its low r side instead of two peaks in the same r space range as seen in the initial $g_{ZnZn}(r)$ function obtained from the SVD solution i.e., the first peak in the latter function most likely represents an over estimate of the intensity in $g_{ZnZn}(r)$ at small r. A comparison between the first peak positions and coordination numbers obtained from the SVD and RMC solutions for the $g_{\alpha\beta}(r)$ functions is made in Table I. A coordination number $\bar{n}_{Cl}^{Cl}=12.1(4)$ is obtained by extending the integration range over the SVD $g_{ClCl}(r)$ function up to 5.22 Å, in agreement with the RMC result. In Table I, a comparison is also

TABLE I. The first peak position in $g_{\alpha\beta}(r)$ and corresponding coordination number for liquid $ZnCl_2$ as obtained by using neutron diffraction (ND), x-ray diffraction (XRD), a combination of XRD and ND, or a combination of diffraction and reverse Monte Carlo (RMC) modeling.

Pair correlation α-β	Peak position (Å)	$\bar{n}_\alpha^\beta$	Integration range (Å)	Temperature (°C)	Method	Reference
Zn-Cl	2.27(2)	4.2(1)	0–2.76	332(5)	ND	Present work
Zn-Zn[a]	3.96(3)	3.8(2)	0–4.54			
Cl-Cl	3.68(3)	10.0(2)	0–4.91			
Zn-Cl	2.27(5)	3.96(1)	0–3.0	332(5)	ND/RMC	Present work
Zn-Zn	3.74(5)	4.20(1)	0–4.5			
Cl-Cl	3.68(5)	12.1(1)	0–5.2			
Zn-Cl	2.27(2)	3.9(1)	0–2.59	328(1)	XRD	Present work
Zn-Cl	2.29(2)	4.3(3)	0–3.0	327	ND	4
Zn-Zn	3.8(1)	4.7(8)	0–4.7			
Cl-Cl	3.71(2)	8.6(5)	0–4.6			
Zn-Cl	2.20	4.1	0–3.10	350	XRD/RMC[b]	9
Zn-Zn	3.85	5.3	0–4.80			
Cl-Cl	3.55	9.6	0–4.70			
Zn-Cl	2.291(2)	4[c]		323	XRD	5
Zn-Zn	3.66(9)	4[c]				
Cl-Cl	3.85(9)	12[c]				
Zn-Cl	2.281(3)	4[c]		350	XRD/ND	8
Zn-Zn	3.92(6)	4[c]				
Cl-Cl	3.69(1)	12[c]				
Zn-Cl	2.28(1)	3.93(6)		330	ND	7
Cl-Cl	3.79(2)[d]					

[a]Values correspond to the light solid (red) curve in Fig. 5.
[b]RMC model obtained by using a single x-ray diffraction pattern.
[c]Input parameter used to model the diffraction data.
[d]Peak position in $r^2 g_{\alpha\beta}(r)$.

made with the parameters obtained from previous diffraction studies of liquid $ZnCl_2$. An extended x-ray absorption fine-structure (EXAFS) spectroscopy study gives $r_{ZnCl}=2.31(1)$ Å with $\bar{n}_{Zn}^{Cl}=4.3(2)$ for the liquid at 340 °C.[68]

B. Glassy $ZnCl_2$ at 25(1) °C

The total structure factors measured for the glassy $ZnCl_2$ samples are shown in Fig. 1(b). The $F(k)$ were used to construct the difference functions $\Delta F_{Cl}(k)$ and $\Delta F(k)$ shown in Fig. 2(b). The corresponding r space functions are given in Fig. 3(b). As for the liquid, the appearance of a peak in $\Delta F_{Cl}(k)$ at $\simeq 1$ Å^{-1}, where $S_{ZnCl}(k)$ receives a positive weighting factor [see Eq. (5)], and a trough in $\Delta F(k)$ at the same k value, where $S_{ZnZn}(k)$ receives a negative weighting factor [see Eq. (6)], is consistent with a contribution to the FSDP in the measured $F(k)$ functions from both Zn-Zn and Zn-Cl correlations. The first peak in $\Delta G_{Cl}(r)$ at 2.28(1) Å has a small r cutoff at 2.09 Å and gives a coordination number $\bar{n}_{Zn}^{Cl}=3.9(1)$. The small r cutoff in $\Delta G(r)$ is at 3.07 Å.

The partial structure factors $S_{\alpha\beta}(k)$ of Fig. 6 were obtained from the total structure factors of Fig. 1(b) by using Eq. (16) and, as shown by comparison with Fig. 4, the error bars are reduced as compared to the liquid. This is consistent with longer counting times for the glass samples and with an absence of a furnace which is necessary for a liquid state experiment. The results show that the largest FSDP appears in $S_{ZnZn}(k)$ and that there is also a notable feature at $\simeq 1$ Å^{-1} in $S_{ZnCl}(k)$. The partial pair distribution functions $g_{\alpha\beta}(r)$ in Fig. 7 were generated by spline fitting the $S_{\alpha\beta}(k)$ functions and Fourier transforming. The first peak in $g_{ZnCl}(r)$ at $r_{ZnCl}=2.27(1)$ Å gives a coordination number $\bar{n}_{Zn}^{Cl}=3.8(3)$, consistent with the results obtained from the difference function $\Delta G_{Cl}(r)$. The first peak in $g_{ClCl}(r)$ at $r_{ClCl}=3.68(1)$ Å gives a ratio $r_{ClCl}/r_{ZnCl}=1.621(8)$ which compares with a ratio of $\sqrt{8/3}=1.633$ for a regular $ZnCl_4$ tetrahedron. The nearest-neighbor Zn-Cl and Cl-Cl peak positions give a Cl-Zn-Cl bond angle of 108(2)° which compares with a regular tetrahedral angle of 109.47°. In Ref. 31 the effect on the first peak in $g_{ZnCl}(r)$ of the finite measurement window function of the diffractometer [$M(k)=1$ for $k \leq k_{max}=23.5$ Å^{-1} and $M(k)=0$ for $k>k_{max}$] was taken into explicit account. This leads to a small sharpening of the first peak but the peak position and coordination number are the same as reported in Table II, within the experimental error.

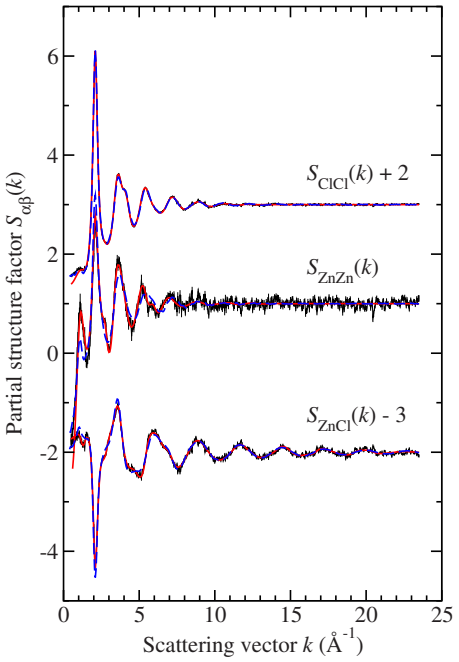

FIG. 6. (Color online) The Faber-Ziman partial structure factors $S_{\alpha\beta}(k)$ for glassy $ZnCl_2$ at 25(1) °C. The vertical bars represent the measured data points with statistical errors and were obtained from the measured total structure factors given in Fig. 1(b) by using Eq. (16). The solid (red) curves are the Fourier back transforms of the corresponding partial pair distribution functions $g_{\alpha\beta}(r)$ given in Fig. 7 after the unphysical oscillations at r values smaller than the distance of closest approach between the centers of two atoms are set to the calculated $g_{\alpha\beta}(r=0)=0$ limit. The broken (blue) curves were obtained from the RMC model and correspond to the total structure factors given by the solid (blue) curves in Fig. 1(b).

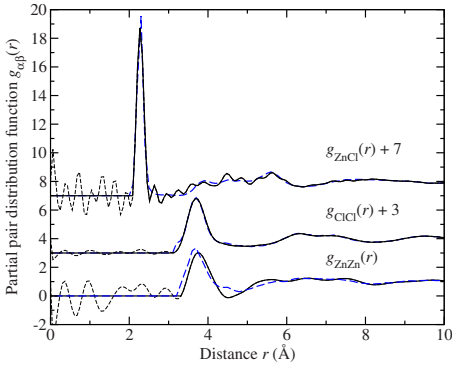

FIG. 7. (Color online) The partial pair distribution functions $g_{\alpha\beta}(r)$ for glassy $ZnCl_2$ at 25(1) °C. The solid (black) curves were obtained by Fourier transforming the measured partial structure factors $S_{\alpha\beta}(k)$ given in Fig. 6 after spline fitting and the thin broken (black) curves at small r show the extent of the unphysical oscillations at r values smaller than the distance of closest approach between the centers of two atoms. The broken (blue) curves are from the RMC model and correspond to the broken (blue) curves in Fig. 6.

Unlike the liquid, $g_{ZnZn}(r)$ for the glass has a single peak at 3.74(1) Å and integration of this peak over the range 3.31–4.42 Å gives a coordination number $\bar{n}^{Zn}_{Zn}=3.8(2)$. Regular edge-sharing tetrahedra would manifest themselves by a peak in $g_{ZnZn}(r)$ at a distance $r_{ZnZn} \leq 2\cos(\gamma/2)r_{ZnCl}$ which, using $r_{ZnCl}=2.27(1)$ Å and $\gamma=109.47°$, gives a maximum distance of $r_{ZnZn}=2.62(1)$ Å. The results are therefore consistent with a network structure made predominantly from corner sharing $ZnCl_4$ tetrahedra[31] where the nearest-neighbor Zn-Zn distance of 3.74(1) Å compares with 3.75–3.77 Å in the anhydrous (delta) phase of crystalline $ZnCl_2$.[10,11] The Zn-Cl and Zn-Zn distances for the glass give a mean Zn-Cl-Zn bond angle of 111(1)°.

The total structure factors $F(k)$, partial structure factors $S_{\alpha\beta}(k)$, and partial pair distribution functions $g_{\alpha\beta}(r)$ obtained from the RMC model for the glass are shown in Figs. 1(b), 6, and 7, respectively. As for the case of the liquid, the Zn-Cl and Cl-Cl pair correlation functions are in good agreement with the measured functions obtained by using the SVD method. There are several discrepancies with respect to the Zn-Zn pair correlation functions which show themselves as a reduction in height of the FSDP in $S_{ZnZn}(k)$ and as a small

TABLE II. The first peak position in $g_{\alpha\beta}(r)$ and corresponding coordination number for glassy $ZnCl_2$ as obtained by using ND, XRD, or a combination of diffraction and RMC modeling.

Pair correlation α-β	Peak position (Å)	$\bar{n}^{\beta}_{\alpha}$	Integration range (Å)	Method	Reference
Zn-Cl	2.27(1)	3.8(3)	0–2.52	ND	Present work
Zn-Zn	3.74(1)	3.8(2)	0–4.42		
Cl-Cl	3.68(1)	11.0(4)	0–4.66		
Zn-Cl	2.29(5)	3.99(1)	0–3.0	ND/RMC	Present work
Zn-Zn	3.67(5)	4.16(1)	0–4.3		
Cl-Cl	3.69(5)	12.2(1)	0–5.0		
Zn-Cl	2.27(2)	4.0(1)	0–2.47	XRD	Present work
Zn-Cl	2.29(1)[a]	3.8		ND	13
Cl-Cl	3.72(1)[a]	9.5			
Zn-Cl	2.32	3.8		XRD	12

[a]Peak position in $rg_{\alpha\beta}(r)$.

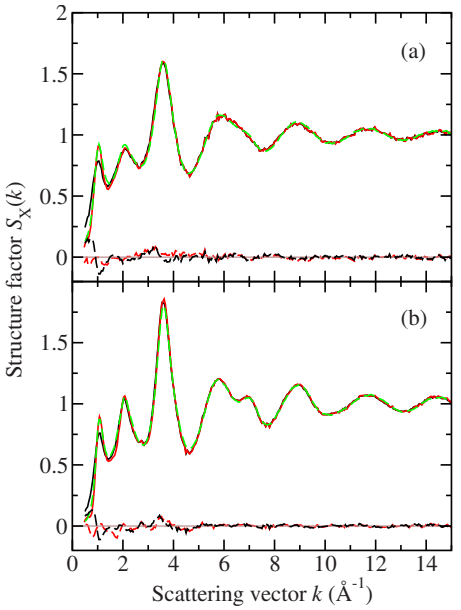

FIG. 8. (Color online) Comparison between the x-ray and neutron-diffraction results for (a) liquid $ZnCl_2$ at $\simeq$330 °C and (b) glassy $ZnCl_2$ at room temperature. For each panel, the broken (green) curve corresponds to the structure factor $S_X(k)$ measured by using x-ray diffraction, the solid dark (black) curve corresponds to the x-ray structure factor $S_X^{rec}(k)$ reconstructed from Eq. (14) using the form factors (Ref. 57) for Zn^{2+} and Cl^- together with the partial structure factors shown by the points with error bars in Fig. 4 or Fig. 6, and the solid light (red) curve corresponds to this data after correction for the resolution function of the neutron diffractometer, ${}^{res}S_X^{rec}(k)$. The broken dark (black) and light (red) curves oscillating about zero give the differences $S_X^{rec}(k)-S_X(k)$ and ${}^{res}S_X^{rec}(k)-S_X(k)$, respectively. The resolution function correction improves agreement between the neutron and x-ray data sets in the region of the FSDP at $\simeq 1$ Å^{-1}.

shift in the first peak position in $g_{ZnZn}(r)$. A comparison between the first peak positions and coordination numbers obtained from the SVD and RMC solutions for the $g_{\alpha\beta}(r)$ functions is made in Table II. A coordination number $\bar{n}_{Cl}^{Cl}=12.0(2)$ is obtained by extending the integration range over the SVD $g_{ClCl}(r)$ function up to 5.22 Å, in agreement with the RMC result. In Table II, a comparison is also made with the parameters obtained from previous diffraction studies on glassy $ZnCl_2$. Early EXAFS spectroscopy studies on the glass give $r_{ZnCl}=2.34(1)$ Å with $\bar{n}_{Zn}^{Cl}=5.1(8)$ (Ref. 69) or $r_{ZnCl}=2.26-2.28$ Å with $\bar{n}_{Zn}^{Cl}\simeq 3$.[70] More recent EXAFS studies are consistent with fourfold coordinated Zn atoms.[71]

C. Comparison with the x-ray diffraction results

The total structure factors $S_X(k)$ measured for liquid $ZnCl_2$ at 328(1) °C and glassy $ZnCl_2$ at room temperature are shown in Fig. 8. The Zn-Cl peak positions and coordination numbers obtained from the corresponding r space functions are listed in Tables I and II where the Zn-Cl coordination numbers were extracted by using the procedure outlined in Ref. 28. Inspection of Fig. 1 shows that the x-ray diffraction patterns for the liquid and glass are very similar to the neutron-diffraction patterns measured for the Zn $^{37}Cl_2$ sample which follows from the similar contrast between the ionic form factors for Zn^{2+} and Cl^- and between the coherent neutron-scattering lengths for Zn and ^{37}Cl nuclei. In the case of x-ray diffraction, the weighting factors for the Zn-Cl, Zn-Zn, and Cl-Cl partial structure factors in $S_X(k)$ [see Eq. (14)] take values of 0.4922, 0.1914, and 0.3164 at $k=0$, respectively. In the case of neutron diffraction, the corresponding weighting factors in $S_N(k)\equiv F(k)/\langle b\rangle+1$ are 0.4979, 0.2189, and 0.2832, respectively, for a sample of Zn $^{37}Cl_2$, where $F(k)$ is defined by Eq. (1).

The x-ray diffraction patterns for the liquid and glass were reconstructed from the partial structure factors measured in the neutron-diffraction experiments. As shown in Fig. 8, the resultant functions, $S_X^{rec}(k)$, do not reproduce the measured x-ray diffraction patterns, $S_X(k)$, in the region of the FSDP at $\simeq 1$ Å^{-1}. This discrepancy can be attributed to the different resolution functions of the instruments used for the diffraction experiments, where the resolution function for the neutron diffractometer D4C is broader than for the x-ray diffractometer on beamline BL04B2 and is asymmetric at smaller k values owing to the so-called umbrella effect.[72–74] To demonstrate this point, a correction for the resolution function was made to the reconstructed x-ray diffraction patterns for the liquid and glass by using the moments method of deconvolution.[74,75] As shown in Fig. 8, this correction improves agreement between the x-ray and neutron-diffraction results, especially in the region of the FSDP. It was checked that the resolution function correction for the x-ray diffractometer is negligible on the scale of the plots shown in Fig. 8.

V. DISCUSSION

A. Comparison between the structure of liquid and glassy $ZnCl_2$

In Fig. 9 a comparison is made between several of the total structure factors measured by neutron diffraction for Zn $^{nat}Cl_2$ samples. Figure 9(a) illustrates the ${}^{nat}F(k)$ functions measured for the liquid at 332(5) °C in the present work and at 330 °C in the work of Allen *et al.*[7] as measured by using the liquids and amorphous diffractometer (LAD) at the ISIS pulsed neutron source. The data sets show discrepancies at several k values that may well result from differences in the resolution function of the instrument used to measure the diffraction patterns, except in the region of the FSDP at $\simeq 1$ Å^{-1} where there appears to be a shift in the level. Application of a resolution function correction[74,75] to the ${}^{nat}F(k)$ function measured in the present work supports the latter observation (see Fig. 9). The present data extrapolate to the correct ${}^{nat}F(k=0)$ limit (see Sec. V B) which suggests that the discrepancy in the low k region results from an inaccurate subtraction of the background scattering in the work of Allen *et al.*[7] Since these data were used by Neuefeind[20] to extract the partial structure factors for the liquid, there will be inaccuracies in these functions at the smallest k values. Figure 9(b) compares the ${}^{nat}F(k)$ functions measured for the glass in the present work and in the work of Desa *et al.*[13] where the diffractometer D4B at the ILL was employed. The

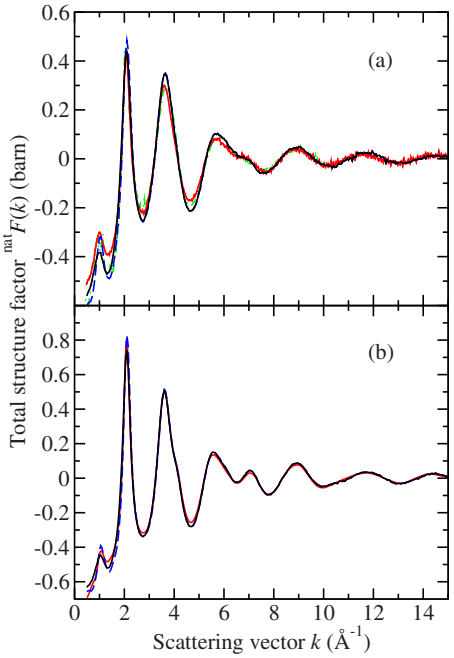

FIG. 9. (Color online) The total structure factor $^{nat}F(k)$ measured by neutron diffraction for liquid and glassy Zn $^{nat}Cl_2$ samples. In (a) the measured functions are shown for the liquid at 332(5) °C from the present work (dark solid (black) curve) and at 330 °C from the work of Allen *et al.* (Ref. 7) [light solid (red) curve with error bars]. Also shown is the total structure factor from the present work corrected for the effect of the diffractometer resolution function [broken (blue) curve]. The measured functions are compared with the total structure factor obtained from the polarizable ion model of Sharma and Wilson (Ref. 36) for the liquid at 327 °C [chained (green) curve]. In (b) the measured functions for the glass are shown from the present work [dark solid (black) curve] and from the work of Desa *et al.* (Ref. 13) [light solid (red) curve with error bars]. Also shown is the total structure factor from the present work corrected for the effect of the diffractometer resolution function [broken (blue) curve].

data sets are in agreement within the experimental error at most k values.

The partial structure factors obtained for the liquid in the present work are compared with the functions measured by Biggin and Enderby[4] in Fig. 10. The $S_{\alpha\beta}(k)$ functions share the same features although the FSDP in the Biggin and Enderby $S_{ZnZn}(k)$ function is somewhat sharper which may be due, in part, to the different resolution functions of the instruments used to make the neutron-diffraction experiments. A comparison of the corresponding partial pair distribution functions is given in Fig. 11. The new results confirm the basic features obtained in the original work of Biggin and Enderby,[4] such as the similar nearest-neighbor Cl-Cl and Zn-Zn distances, although there are differences in detail.

The configurations obtained from the RMC models for the liquid and glass were analyzed to give additional information on the atomic configurations. The relative percentages of $ZnCl_3$, $ZnCl_4$, and $ZnCl_5$ units, evaluated by using a Zn-Cl cut-off distance of 3.0 Å, are 14.7%, 74.2%, and 11.1% for the liquid and 5.5%, 90.2%, and 4.3% for the glass, respectively, giving a mean coordination number of $\bar{n}_{Zn}^{Cl}$=3.96 for

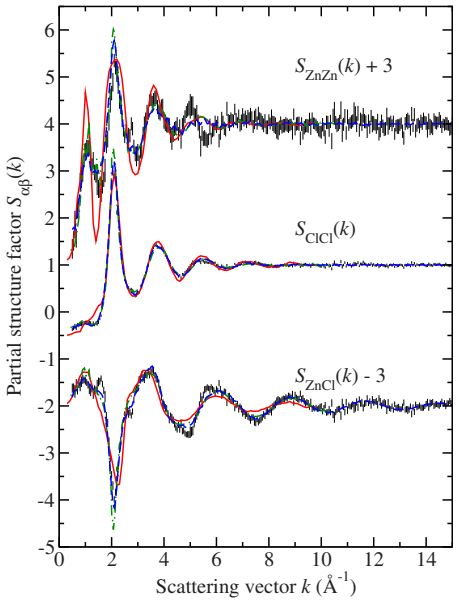

FIG. 10. (Color online) Comparison between the Faber-Ziman partial structure factors $S_{\alpha\beta}(k)$ for liquid $ZnCl_2$ as measured at 332(5) °C in the present work (points with vertical error bars) and at 327 °C in the work of Biggin and Enderby (Ref. 4) [solid (red) curves]. The broken (blue) curves are from the RMC model for the liquid at 332 °C and the chained (green) curves are from the polarizable ion model of Sharma and Wilson for the liquid at 327 °C (Ref. 36).

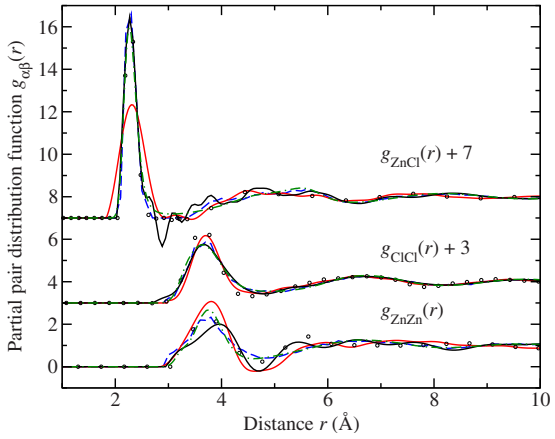

FIG. 11. (Color online) Comparison between the partial pair distribution functions $g_{\alpha\beta}(r)$ for liquid $ZnCl_2$ as measured at 332(5) °C in the present work [solid (black) curves] and at 327 °C in the work of Biggin and Enderby (Ref. 4) [light solid (red) curves]. The first peak in the latter $g_{ZnCl}(r)$ function is broadened by comparison with the present work due to truncation of the Biggin and Enderby $S_{ZnCl}(k)$ function at a smaller k_{max} value of 10 Å^{-1} prior to Fourier transformation. The peak at 2.97 Å in $g_{ZnZn}(r)$ for the present work has been removed (see the text). The broken (blue) curves are from the present RMC model for the liquid at 332 °C, the open circles are from the model of Neuefeind (Ref. 20) for the liquid at 327 °C as obtained by combining x-ray and neutron-diffraction data, and the chained (green) curves are from the polarizable ion model of Sharma and Wilson for the liquid at 327 °C (Ref. 36).

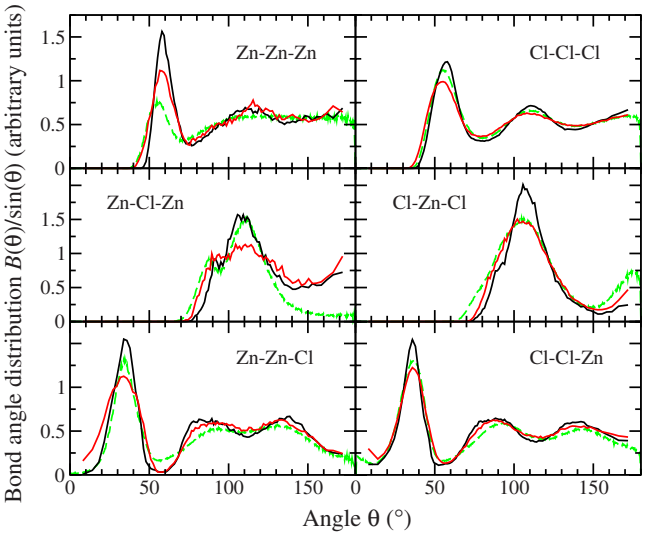

FIG. 12. (Color online) The bond angle distributions obtained from the RMC models for liquid $ZnCl_2$ at 332(5) °C [light solid (red) curves] and glassy $ZnCl_2$ at 25(1) °C [dark solid (black) curves]. The broken (green) curves show the bond angle distributions obtained from the polarizable ion model of Sharma and Wilson for the liquid at 327 °C (Ref. 36). Each of the latter has been scaled to best match the corresponding RMC generated bond angle distribution for the liquid.

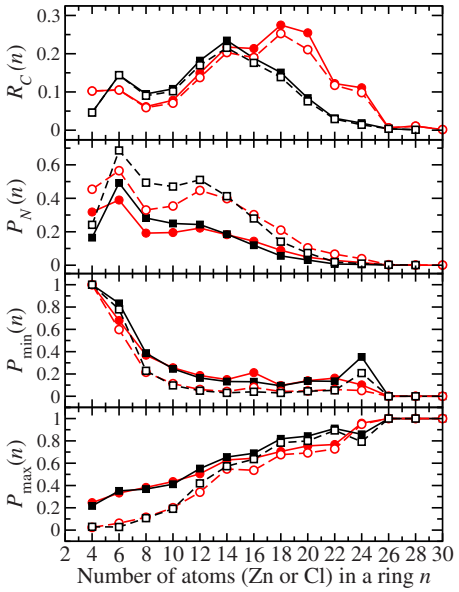

FIG. 13. (Color online) The connectivity profiles for the RMC models of liquid $ZnCl_2$ at 332(5) °C [light (red) circles] and glassy $ZnCl_2$ at 25(1) °C [dark (black) squares] as calculated by using the RINGS code (Ref. 77) within ISAACS (Ref. 78). The solid symbols and curves correspond to the results obtained when using both Zn and Cl atoms as the starting point for a shortest path search and the open symbols and broken curves correspond to the results obtained when using only Zn atoms as the starting point for a shortest path search. The absence of symbols for odd membered rings implies an absence of these configurations in the models.

the liquid and $\bar{n}_{Zn}^{Cl}=3.99$ for the glass. The bond angle distributions shown in Fig. 12 were obtained by using additional Zn-Zn and Cl-Cl cut-off values of 4.5 Å and 5.2 Å for the liquid and 4.3 Å and 5.0 Å for the glass, respectively. Each bond angle distribution $B(\theta)$ is proportional to the number of bonds between angles of θ and $\theta+\Delta\theta$ which depends on the solid angle subtended at that value of θ. The latter is proportional to sin θ and it is therefore appropriate to remove its effect by plotting the distribution $B(\theta)/\sin(\theta)$ so that peaks are not distorted, e.g., a finite bond angle distribution at $\theta \simeq 180°$ will not be artificially suppressed.[76]

The connectivity profiles shown in Fig. 13 were evaluated by employing the Rigorous Investigation of Networks Generated using Simulation (RINGS) code[77] within the Interactive Structure Analysis of Amorphous and Crystalline Systems (ISAACS) program,[78] using the same cut-off distances as for the bond angle distributions. The analysis was performed by making a shortest path search for rings containing a maximum of 30 atoms using either (i) each and every atom as a starting point to initiate a shortest path search or (ii) only Zn atoms as a starting point to initiate a shortest path search. The possibility of homopolar bonds was not excluded from the searching procedure. $R_C(n)$ is the number of rings containing n atoms (Zn or Cl) that are found, normalized to the total number of atoms in the model. $P_N(n)$ is the number of atoms that can be used as a starting point to initiate a search for at least one ring containing n atoms, normalized to the total number of atoms in the model that were used to initiate a search. The latter is not, in general, equal to the number of atoms in an n-fold ring normalized to the total number of atoms in the model that were used to initiate a search, $R_N(n)$, because an atom in a particular ring cannot necessarily be used as the origin of search for finding that ring via a shortest path algorithm.[77] For a given atom of a specific chemical species in an n-fold ring, $P_{min}(n)$ gives the probability that this ring constitutes the shortest closed path that can be found by using this atom as a starting point to initiate a search and, conversely, $P_{max}(n)$ gives the probability that this ring constitutes the longest closed path that can be found by using this atom as a starting point to initiate a search.

The maximum in the Cl-Zn-Cl bond angle distribution at ≈106° in the case of the glass, near to the angle of 109.47° expected for a regular tetrahedron, is shifted to a smaller angle in the case of the liquid. The Zn-Cl-Zn bond angle distribution shows a peak at ≈106° with a shoulder at ≈92° which is broadened in the case of the liquid. A Zn-Cl-Zn bond angle of 106° with a Zn-Cl bond distance of 2.27 Å corresponds to a Zn-Zn distance of 3.63 Å, i.e., the peak in $g_{ZnZn}(r)$ at ≈3.7 Å arises from corner sharing tetrahedra. However, a Zn-Cl-Zn bond angle of ≈90° points to the presence of distorted edge-sharing tetrahedra, with a Zn-Zn distance of 3.21 Å. These configurations account for the shoulder on the small r side of the first peak in $g_{ZnZn}(r)$ for the liquid (see Fig. 5) and lead to a small shoulder at ≈90° in the Cl-Zn-Cl bond angle distribution (according to Ref. 50 the Cl-Zn-Cl bond angle for bridging connections is 93.8° in the vapor phase). The fraction of fourfold coordinated Zn atoms in corner and edge-sharing configurations was estimated at 63% and 37% for the liquid and at 82% and 18% for the glass, respectively, by using the bond properties code within ISAACS.[78] No face sharing conformations were observed. The existence of both corner and edge-sharing tetrahedra in liq-

uid and glassy $ZnCl_2$ is supported by Raman spectroscopy experiments[23] and by several models for the liquid.[9,21,36,79] The peak in the Zn-Zn-Zn bond angle distribution at ≈60° is related to a peak in $R_C(n)$ shown in Fig. 13 and corresponds to rings containing three Zn and three Cl atoms (see below).

In Fig. 13 the absence of odd membered rings is characteristic of a chemically ordered network (Zn-Cl-Zn-Cl connections), as befits an ionic system. The profile of $R_C(n)$ indicates a broad distribution of ring sizes with a minimum ring size of $n=4$ atoms, corresponding to the occurrence of edge-sharing tetrahedra, and with maxima at $n=6$ and at either $n=14$ (glass) or $n=18$ (liquid). The $P_N(n)$ values show that the number of atoms that can be used as the origin of search for sixfold rings is large compared to the number of atoms that can be used as the origin of search for, e.g., 14- or 18-fold rings. Sixfold rings containing three Zn and three Cl atoms are therefore a significant feature of both the liquid and glass networks.[77] The $P_{\min}(n=4)=1$ value implies that an atom within a fourfold ring cannot be used as the origin of search for a smaller ring, consistent with edge-sharing tetrahedra forming the shortest closed paths. The $P_{\max}(n=4) \simeq 0.23$ value found for the liquid and glass when using both Zn and Cl atoms as the origin of search means that there is a ≃23% probability that an atom at the origin of search within a fourfold ring is in the largest ring that can be found for that atom, i.e., there is a ≃77% chance that this atom can also be used as the origin of search for a ring with $n>4$. The $P_{\max}(n=4)$ value drops to ≃0.02 for the liquid and glass when using only Zn atoms as the origin of search. This means that there is a ≃98% chance that a Zn atom within a fourfold ring can also be used as the origin of search for a ring with $n>4$, consistent with the notion that Zn atoms act as "network forming" nodes.[77]

The packing fraction of Cl atoms can be estimated from their diameter of 3.68 Å (see Tables I and II) and from the measured number density (see Sec. III B) and is 0.583(5) for the liquid at 332 °C and 0.625(2) for the glass at 25 °C. These values compare with a packing fraction of ≈0.64 for a dense random packing of hard spheres.[80,81] Indeed, the structure of vitreous $ZnCl_2$ is often described in terms of a distorted random close-packed array of Cl atoms with the Zn atoms occupying the tetrahedral holes and arranged in such a way as to maximize the number of corner sharing $ZnCl_4$ tetrahedra.[13] To examine this feature of the structure in more detail, hard sphere Monte Carlo simulations were made using 2000 particles with a number density set to two thirds the measured number density of the liquid or glass with a nearest-neighbor cut-off distance of 3.5 Å, roughly equal to the diameter of a chloride ion.[82] The resultant bond angle distributions, obtained by using large r cut-off values of 5.0 and 4.9 Å for the liquid and glass, respectively, are compared to the RMC generated Cl-Cl-Cl bond angle distributions in Fig. 14. A comparison is also made with the bond angle distribution generated from the large 7934 sphere random close packing model of Bernal and co-workers having a packing fraction of 0.6366(4).[81,83] As illustrated in Fig. 14, the hard sphere bond angle distributions show the same overall features as the Cl-Cl-Cl bond angle distributions with peaks at ≈60° and ≈110°. The peak at ≈60° in the Cl-Cl-Cl distributions is, however, broader than in the corresponding hard sphere distributions which is consistent with a less regular arrangement of the nearest-neighbor Cl atoms in liquid and glassy $ZnCl_2$. The peak at ≈60° in the distribution for the random close packing model is especially sharp in keeping with the high packing fraction and absence of thermal effects.

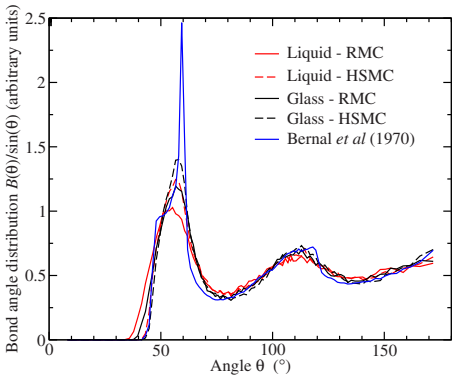

FIG. 14. (Color online) Comparison between the Cl-Cl-Cl bond angle distributions for liquid [light solid (red) curve] and glassy [dark solid (black) curve] $ZnCl_2$ as generated by RMC (see Fig. 12) with the bond angle distributions obtained from hard sphere Monte Carlo (HSMC) simulations of the liquid [light broken (red) curve] and glass [dark broken (black) curve] (see the text) and with the bond angle distribution obtained from the large 7934 sphere random close packing model of Bernal and co-workers (Refs. 81 and 83) [dark solid (blue) curve with sharp peak].

B. Structure of liquid and glassy $ZnCl_2$ within the Bhatia-Thornton formalism

The Bhatia-Thornton partial structure factors $S_{IJ}^{\mathrm{BT}}(k)$ and the corresponding partial pair distribution functions $g_{IJ}^{\mathrm{BT}}(r)$ for liquid and glassy $ZnCl_2$ are shown in Figs. 15 and 16, respectively. The position and width of the first two peaks in reciprocal space are listed in Table III. As discussed in Sec. II B, the weighting factor matrix used to obtain the $S_{IJ}^{\mathrm{BT}}(k)$ functions is better conditioned than the matrix used to obtain the $S_{\alpha\beta}(k)$ functions and accounts for the reduction in size of the error bars for $S_{CC}^{\mathrm{BT}}(k)$ compared to $S_{\mathrm{ZnZn}}(k)$ (see Figs. 4 and 6). In reciprocal space, all three partial structure factors for the liquid have an FSDP at ≃1 $\mathrm{Å}^{-1}$ and a principal peak or trough at ≃2.09 $\mathrm{Å}^{-1}$. The corresponding peaks in the $S_{IJ}^{\mathrm{BT}}(k)$ functions for the glass also share common positions but the height of the principal peak is increased relative to the FSDP.

The FSDP in $S_{CC}^{\mathrm{BT}}(k)$ for network glass forming MX_2 systems arises from concentration fluctuations on an intermediate length scale.[18] As shown by Eq. (12), the FSDP indicates a preference for like atom correlations on the corresponding length scale in real space and is usually attributable to $S_{MM}(k)$.[18,19] The origin of the FSDP in $S_{CC}^{\mathrm{BT}}(k)$ has been the subject of much debate.[35,84–95] For example, in the case of a simple ionic model for an MX_2 system with pointlike charges $S_{CC}^{\mathrm{BT}}(k)=c_M c_X S_{ZZ}(k)$, where $S_{ZZ}(k)$ is the charge-charge partial structure factor so that an FSDP in $S_{CC}^{\mathrm{BT}}(k)$ equates to a nonuniformity in the charge distribution on the scale of the

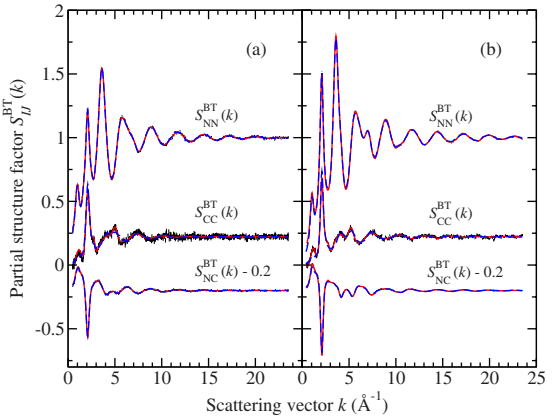

FIG. 15. (Color online) The Bhatia-Thornton partial structure factors $S^{BT}_{IJ}(k)$ for (a) liquid $ZnCl_2$ at 332(5) °C and (b) glassy $ZnCl_2$ at 25(1) °C. The vertical bars represent the measured data points with statistical errors and were obtained from the measured total structure factors given in Fig. 1 by using Eq. (16). The solid (red) curves are the Fourier back transforms of the corresponding partial pair distribution functions $g^{BT}_{IJ}(r)$ given in Fig. 16 after the unphysical oscillations at r values smaller than the distance of closest approach between the centers of two atoms are set to the calculated $g^{BT}_{IJ}(r=0)=0$ limit. The broken (blue) curves are from the RMC model and correspond to the broken (blue) curves in Fig. 16.

intermediate range order.[18] However, first-principles molecular-dynamics simulations in which the valence electron density is taken into account show an absence of charge fluctuations on this scale irrespective of whether there is an FSDP in $S^{BT}_{CC}(k)$, i.e., charge and structural ordering need to be distinguished.[88,89] In the case of $GeSe_2$ the observation of an FSDP in $S^{BT}_{CC}(k)$ by neutron diffraction[24–27] has led to the incorporation of improved energy functionals in first-

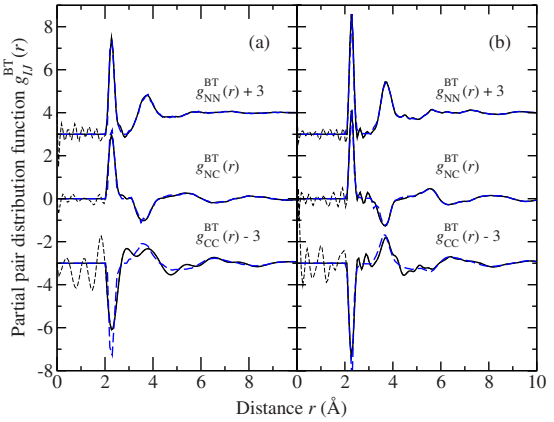

FIG. 16. (Color online) The Bhatia-Thornton partial pair distribution functions $g^{BT}_{IJ}(r)$ for (a) liquid $ZnCl_2$ at 332(5) °C and (b) glassy $ZnCl_2$ at 25(1) °C. The solid (black) curves were obtained by Fourier transforming the measured partial structure factors $S^{BT}_{IJ}(k)$ given in Fig. 15 after spline fitting and the thin broken (black) curves at small r show the extent of the unphysical oscillations at r values smaller than the distance of closest approach between the centers of two atoms. The broken (blue) curves are from the RMC model and correspond to the broken (blue) curves in Fig. 15.

TABLE III. The position of the first sharp diffraction peak k_{FSDP} and principal peak k_{PP} in the measured Bhatia-Thornton partial structure factors $S^{BT}_{IJ}(k)$ together with the half width at half maximum of these peaks Δk_{FSDP} and Δk_{PP}, respectively.

Phase	Pair correlation I-J	k_{FSDP} (Å^{-1})	Δk_{FSDP} (Å^{-1})	k_{PP} (Å^{-1})	Δk_{PP} (Å^{-1})
Liquid	N-N	1.00(2)	0.205(10)	2.09(2)	0.23(1)
	C-C	1.14(2)	0.275(10)	2.11(2)	0.24(1)
	N-C	1.07(2)	0.205(10)	2.09(2)	0.21(1)
Glass	N-N	1.08(2)	0.19(1)	2.09(2)	0.19(1)
	C-C	1.01(2)	0.225(10)	2.10(2)	0.19(1)
	N-C	1.14(2)	0.20(1)	2.11(2)	0.16(2)

principles molecular-dynamics simulations which lead to an enhanced charge transfer between the chemical species.[85,86,94,96]

Three classes of network system have been identified by first-principles molecular-dynamics simulations where (1) there is perfect chemical order and no FSDP in $S^{BT}_{CC}(k)$, (2) a moderate number of defects in an otherwise chemically ordered network and an FSDP in $S^{BT}_{CC}(k)$, or (3) much chemical disorder featuring a rich variety of structural motifs and no FSDP in $S^{BT}_{CC}(k)$.[88,89] In the case of $GeSe_2$, the height of the FSDP has been correlated with the presence of Ge atoms in fourfold rings, i.e., with the presence of edge-sharing configurations containing two Ge and two Se atoms.[35,90,91,93,97] Systematic investigations are needed to see whether the FSDP observed in $S^{BT}_{CC}(k)$ for liquid and glassy $ZnCl_2$ has a similar origin.

The pair distribution functions $g^{BT}_{IJ}(r)$ show ordering that extends to large distances and which is associated not with the FSDP but with the principal peak in the corresponding $S^{BT}_{IJ}(k)$ functions.[31] This can be readily observed by plotting the functions $rh^{BT}_{NN}(r) \equiv r[g^{BT}_{NN}(r)-1]$, $rh^{BT}_{NC}(r) \equiv rg^{BT}_{NC}(r)$, and $rh^{BT}_{CC}(r) \equiv rg^{BT}_{CC}(r)$ as extensively discussed elsewhere for glassy $ZnCl_2$ and other MX_2 network glass forming systems.[19,31,98–101] At large distances, the behavior of these pair correlation functions can be represented by an exponentially decaying oscillatory function of the form $rh^{BT}_{IJ}(r)=|A_{IJ}|\exp(-a_0 r)\cos(a_1 r-\theta_{IJ})$, where A_{IJ} is an amplitude, θ_{IJ} is a phase, the wavelength of the oscillations is given by $2\pi/a_1$, and the decay length is given by a_0^{-1}. For many network glass forming systems it is found that $a_1 \simeq k_{PP}$ and $a_0 \simeq \Delta k_{PP}$, where Δk_{PP} is the half width at half maximum of the principal peak.[19,100] As indicated by the parameters listed in Table III, the pair correlation functions for a given phase have comparable wavelengths of oscillation and comparable decay lengths, the correlations decaying more rapidly with distance in the case of the liquid in accordance with the larger width of the principal peak.

For an ionic interaction model the $k=0$ limiting values for the N-N and N-C Bhatia-Thornton partial structure factors are obtained from the expressions $S^{BT}_{NN}(k=0)=n_0 k_B T \kappa_T$ and $S^{BT}_{NC}(k=0)=0$, where k_B is the Boltzmann constant, T is the absolute temperature, and κ_T is the isothermal compressibility.[98,100] The small k behavior of the C-C partial

structure factor is given by $S_{CC}^{BT}(k)=\Lambda_D^2 k^2$, where Λ_D is the Debye screening length

$$\Lambda_D^{-2}=\frac{4\pi n_0}{k_B T\epsilon}\sum_\alpha c_\alpha (Z_\alpha e)^2, \tag{19}$$

$\epsilon \equiv 4\pi\epsilon_r\epsilon_0$, ϵ_r is the dimensionless relative dielectric constant, ϵ_0 is the vacuum permittivity, $Z_\alpha e$ is the charge on chemical species α, and e is the elementary charge. The present data do not access small enough k values with sufficient accuracy to enable a thorough experimental investigation of the limiting behavior of the $S_{IJ}^{BT}(k)$ functions.[98] However, we note that sound velocity measurements give an adiabatic compressibility $\kappa_S=3.89\times10^{-10}$ m^2 N^{-1} for molten $ZnCl_2$ at 332 °C and the ratio of the constant pressure to constant volume heat capacities $\gamma=C_p/C_v=1.04$ at 400 °C.[102] Since $\kappa_T=\gamma\kappa_S\simeq4.05\times10^{-10}$ m^2 N^{-1} and $n_0=0.0335$ Å^{-3} it follows that $S_{NN}^{BT}(k=0)=0.1133$ at 332 °C. By using Eq. (9), a limiting value $F(k=0)=\langle b\rangle^2 S_{NN}^{BT}(k=0)-(c_{Zn}b_{Zn}^2+c_{Cl}b_{Cl}^2)=-0.641$ barn is calculated for a sample of Zn $^{nat}Cl_2$. By plotting the $^{nat}F(k)$ data of Fig. 9(a) as a function of k^2 and fitting a straight line to the small k region, a limiting value of $^{nat}F(k=0)=-0.631(4)$ barn is obtained from the present work for the liquid at 332(5) °C whereas a limiting value of $^{nat}F(k=0)=-0.573(6)$ barn is obtained from the work of Allen *et al.*[7] for the liquid at 330 °C, i.e., the present work gives a result that is in better agreement with the thermodynamic limit.

We also note that in order to calculate the Debye screening length given by Eq. (19), ϵ_r is often set to the "high-frequency" dielectric constant ϵ_∞ which can be obtained by measuring the refractive index n of the medium at optical frequencies where $n^2=\epsilon_\infty$.[98] The refractive index of liquid $ZnCl_2$ at 320 °C measured using light of wavelength 0.5461 μm is 1.588(1) (Ref. 103) which gives an estimate of $\Delta_D^2=0.0108$ Å^2 for molten $ZnCl_2$ at 332 °C.

C. Comparison of the liquid structure with computational models

Several computational models of liquid $ZnCl_2$ have been developed[9,15,35,36,79,104–113] and a recent discussion is given in Ref. 36. Madden and Wilson focused on a PIM for the atomic interactions which reproduces experimental features such as the relatively short nearest-neighbor Zn-Zn distance and an FSDP in the Zn-Zn partial structure factor at ≈1 Å^{-1}, thereby demonstrating the importance of polarization effects.[15,16] A comparison between the total structure factor $^{nat}F(k)$ for the liquid obtained from the present work and from the most recent PIM (Refs. 35 and 36) is shown in Fig. 9(a) while comparisons between the corresponding $S_{\alpha\beta}(k)$ and $g_{\alpha\beta}(r)$ functions are shown in Figs. 10 and 11, respectively. The Cl-Cl and Zn-Cl pair correlation functions obtained from the SVD, RMC, and PIM methods are all in agreement within the experimental error in both reciprocal and real space. There is also good agreement between the Zn-Zn pair correlation functions obtained from these methods although the Zn-Zn nearest-neighbor distance obtained from the SVD $g_{ZnZn}(r)$ function is rather long, in accordance with the discussion of Sec. IV A. The relative percentages of $ZnCl_3$, $ZnCl_4$, $ZnCl_5$, and $ZnCl_6$ units is 14.7%, 74.2%, 11.1%, and 0% for the RMC model (Sec. V A) and 0%, 73.7%, 24.1%, and 2.2% for the PIM, i.e., although both models give almost the same number of tetrahedral units there is a difference between the relative number of other structural units. As shown in Fig. 12, the bond angle distributions obtained from the RMC method and the PIM are in fair accord. For example, the Cl-Cl-Cl bond angle distributions are almost identical and there is a peak at ≈88° in the Zn-Cl-Zn bond angle distribution for the PIM which is consistent with the presence of edge-sharing tetrahedra. In the PIM, the fraction of Zn atoms at the center of two edge sharing units i.e. belonging to two fourfold rings (the "Zn(2)" sites referred to in Ref. 93) is ≈27%.[36] It will be interesting to see whether the discrepancies between experiment and theory can be resolved by parametrizing potential-energy functions using the results obtained from density-functional theory.[92]

VI. CONCLUSIONS

The partial structure factors for liquid and glassy $ZnCl_2$ have been obtained from the diffraction patterns measured by using the method of isotope substitution in neutron diffraction by employing both the SVD and RMC procedures. The agreement between the results is good in the case of the Cl-Cl and Zn-Cl pair correlation functions but is not as robust in the case of the Zn-Zn pair correlation functions. This is anticipated on the basis of the conditioning of the matrix given in Eq. (2) which is discussed in Sec. II B. The statistical errors are larger for the liquid relative to the glass since the counting times were smaller and the scattering from a furnace needs to be subtracted from the intensity measured for a liquid sample. The RMC solution for liquid $ZnCl_2$ is preferred over the SVD solution because it does not have a peak at $r=2.97$ Å in $r_{ZnZn}(r)$, a feature which is not expected on the basis of the measured real-space difference functions and which is difficult to rationalize in terms of models based on edge and corner sharing tetrahedral units (see Sec. IV A). All RMC solutions are guaranteed to be consistent with a three-dimensional arrangement of atoms, although the modeling procedure tends to produce the most disordered structure that is consistent with the data and applied constraints.[34] Notwithstanding, the neutron-diffraction results for the liquid and glass are in excellent agreement with high-energy x-ray diffraction data in which the Zn-Zn correlations have a large weighting factor, once a correction for the resolution function of the neutron diffractometer is made.

The results for liquid and glassy $ZnCl_2$ obtained from the SVD and RMC methods support the formation of a network made predominantly from corner sharing $ZnCl_4$ tetrahedra. There is also a small number of edge-sharing configurations that are more numerous in the liquid. The tetrahedra organize to give a nearest-neighbor Zn-Zn distance that is comparable to the nearest-neighbor Cl-Cl distance, in agreement with the previous neutron-diffraction results of Biggin and Enderby[4] for the liquid phase. On an intermediate length scale, the organization of the tetrahedra gives rise to an FSDP in the Zn-Zn partial structure factor at ≃1 Å^{-1} with a smaller fea-

ture at the same position in the Zn-Cl partial structure factor. The results for liquid $ZnCl_2$ are consistent with the premise that the fragility of tetrahedral glass forming MX_2 liquids is correlated with the presence of edge-sharing units, these conformations being absent in strong liquids such as SiO_2 and GeO_2.[29]

ACKNOWLEDGMENTS

We would like to thank Robert McGreevy (ISIS) for procuring the chlorine isotopes, John Rowden (Bristol) and Phil Jones (Bath) for making the glassware for the sample preparation associated with the neutron and x-ray diffraction experiments, respectively, Alex Hannon (ISIS) for an energy dispersive neutron-diffraction experiment on one of our test samples, Pierre Palleau (ILL) for help with the neutron-diffraction experiments, Adrian Barnes (Bristol), Karl Ludwig, Jr. (Boston) and Arthur Bienenstock (Stanford) for helpful discussions on SVD, Spencer Howells (ISIS) for masterminding the deconvolution procedure, Dave Keen (ISIS), Matt Tucker (ISIS) and László Temleitner (SPring-8) for helpful discussions on bond angle distributions, Sébastien Le Roux (Strasbourg) and Carlo Massobrio (Strasbourg) for advice on ring statistics, Mark Wilson (Oxford) for many useful discussions and for providing his data sets for the PIM, Jörg Neuefeind (SNS) for supplying his results for liquid $ZnCl_2$, and John Finney (UCL) for providing the coordinates for the large random close packing model. Phil Salmon thanks the ILL for a visiting scientist position during which this work was written up, and Takeshi Usuki thanks the Japan Society for the Promotion of Science (JSPS) for supporting his stay in Bath. We also thank the EPSRC for financial support and for providing its Chemical Database Service.

*Present address: Department of Material and Biological Chemistry, Faculty of Science, Yamagata University, 1-4-12 Koshirakawa, Yamagata 990-8560, Japan.

[1] C. A. Angell and J. Wong, J. Chem. Phys. **53**, 2053 (1970).
[2] C. A. Angell, Science **267**, 1924 (1995).
[3] J. C. Wasse and P. S. Salmon, J. Phys.: Condens. Matter **10**, 8139 (1998).
[4] S. Biggin and J. E. Enderby, J. Phys. C **14**, 3129 (1981).
[5] R. Triolo and A. H. Narten, J. Chem. Phys. **74**, 703 (1981).
[6] Y. Takagi and T. Nakamura, Nippon Kagaku Kaishi 928 (1982).
[7] D. A. Allen, R. A. Howe, N. D. Wood, and W. S. Howells, J. Chem. Phys. **94**, 5071 (1991).
[8] J. Neuefeind, K. Tödheide, A. Lemke, and H. Bertagnolli, J. Non-Cryst. Solids **224**, 205 (1998).
[9] A. Bassen, A. Lemke, and H. Bertagnolli, Phys. Chem. Chem. Phys. **2**, 1445 (2000).
[10] J. Brynestad and H. L. Yakel, Inorg. Chem. **17**, 1376 (1978).
[11] H. L. Yakel and J. Brynestad, Inorg. Chem. **17**, 3294 (1978).
[12] M. Imaoka, Y. Konagaya, and H. Hasegawa, J. Ceram. Soc. Jpn. **79**, 97 (1971).
[13] J. A. E. Desa, A. C. Wright, J. Wong, and R. N. Sinclair, J. Non-Cryst. Solids **51**, 57 (1982).
[14] E. Kartini, M. F. Collins, F. Mezei, and E. C. Svensson, Physica B **241-243**, 909 (1997).
[15] M. Wilson and P. A. Madden, J. Phys.: Condens. Matter **5**, 6833 (1993).
[16] P. A. Madden and M. Wilson, Chem. Soc. Rev. **25**, 339 (1996).
[17] A. B. Bhatia and D. E. Thornton, Phys. Rev. B **2**, 3004 (1970).
[18] P. S. Salmon, Proc. R. Soc. London, Ser. A **437**, 591 (1992).
[19] P. S. Salmon, J. Phys.: Condens. Matter **19**, 455208 (2007).
[20] J. Neuefeind, Phys. Chem. Chem. Phys. **3**, 3987 (2001).
[21] A. K. Soper, Pramana J. Phys. **63**, 41 (2004).
[22] A. K. Soper, Phys. Rev. B **72**, 104204 (2005).
[23] S. N. Yannopoulos, A. G. Kalampounias, A. Chrissanthopoulos, and G. N. Papatheodorou, J. Chem. Phys. **118**, 3197 (2003).
[24] I. T. Penfold and P. S. Salmon, Phys. Rev. Lett. **67**, 97 (1991).
[25] I. Petri, P. S. Salmon, and H. E. Fischer, Phys. Rev. Lett. **84**, 2413 (2000).
[26] P. S. Salmon and I. Petri, J. Phys.: Condens. Matter **15**, S1509 (2003).
[27] P. S. Salmon, J. Non-Cryst. Solids **353**, 2959 (2007).
[28] A. Zeidler, J. W. E. Drewitt, P. S. Salmon, A. C. Barnes, W. A. Crichton, S. Klotz, H. E. Fischer, C. J. Benmore, S. Ramos, and A. C. Hannon, J. Phys.: Condens. Matter **21**, 474217 (2009).
[29] M. Wilson and P. S. Salmon, Phys. Rev. Lett. **103**, 157801 (2009).
[30] H. E. Fischer, G. J. Cuello, P. Palleau, D. Feltin, A. C. Barnes, Y. S. Badyal, and J. M. Simonson, Appl. Phys. A **74**, s160 (2002).
[31] P. S. Salmon, R. A. Martin, P. E. Mason, and G. J. Cuello, Nature (London) **435**, 75 (2005).
[32] K. F. Ludwig, Jr., W. K. Warburton, L. Wilson, and A. I. Bienenstock, J. Chem. Phys. **87**, 604 (1987).
[33] R. L. McGreevy and L. Pusztai, Mol. Simul. **1**, 359 (1988).
[34] R. L. McGreevy, J. Phys.: Condens. Matter **13**, R877 (2001).
[35] B. K. Sharma and M. Wilson, Phys. Rev. B **73**, 060201(R) (2006).
[36] B. K. Sharma and M. Wilson, J. Phys.: Condens. Matter **20**, 244123 (2008).
[37] H. E. Fischer, A. C. Barnes, and P. S. Salmon, Rep. Prog. Phys. **69**, 233 (2006).
[38] T. E. Faber and J. M. Ziman, Philos. Mag. **11**, 153 (1965).
[39] V. F. Sears, Neutron News **3**, 26 (1992).
[40] C. L. Lawson and R. J. Hanson, *Solving Least Squares Problems* (Prentice-Hall, Englewood Cliffs, NJ, 1974).
[41] G. E. Forsythe, M. A. Malcolm, and C. B. Moler, *Computer Methods for Mathematical Computations* (Prentice-Hall, Englewood Cliffs, NJ, 1977).
[42] W. H. Press, S. A. Teukolsky, W. T. Vetterling, and B. P. Flannery, *Numerical Recipes in Fortran 77*, 2nd ed. (Cambridge University Press, Cambridge, 1992).
[43] C. D. Meyer, *Matrix Analysis and Applied Linear Algebra* (SIAM, Philadelphia, 2000).
[44] D. S. Watkins, *Fundamentals of Matrix Computations*, 2nd ed. (Wiley, New York, 2002).
[45] F. G. Edwards, J. E. Enderby, R. A. Howe, and D. I. Page, J. Phys. C **8**, 3483 (1975).

[46] J. R. Westlake, *A Handbook of Numerical Matrix Inversion and Solution of Linear Equations* (Wiley, New York, 1968).
[47] M. Hargittai, J. Tremmel, and I. Hargittai, Inorg. Chem. **25**, 3163 (1986).
[48] M. Kaupp and H. G. von Schnering, Inorg. Chem. **33**, 4718 (1994).
[49] M. Hargittai, Struct. Chem. **16**, 33 (2005).
[50] K. J. Donald, M. Hargittai, and R. Hoffmann, Chem.-Eur. J. **15**, 158 (2009).
[51] S. F. Mughabghab, *Atlas of Neutron Resonances: Resonance Parameters and Thermal Cross Sections* $Z=1-100$, 5th ed. (Elsevier, Amsterdam, 2006).
[52] H. Bertagnolli, P. Chieux, and M. D. Zeidler, Mol. Phys. **32**, 759 (1976).
[53] J. F. Jal, C. Mathieu, P. Chieux, and J. Dupuy, Philos. Mag. B **62**, 351 (1990).
[54] P. S. Salmon, J. Phys. F: Met. Phys. **18**, 2345 (1988).
[55] P. S. Salmon, S. Xin, and H. E. Fischer, Phys. Rev. B **58**, 6115 (1998).
[56] S. Kohara, M. Itou, K. Suzuya, Y. Inamura, Y. Sakurai, Y. Ohishi, and M. Takata, J. Phys.: Condens. Matter **19**, 506101 (2007).
[57] E. N. Maslen, A. G. Fox, and M. A. O'Keefe, in *International Tables for Crystallography*, 2nd ed., Vol. C, edited by A. J. C. Wilson and E. Prince (Kluwer, Dordrecht, 1999), p. 548, Sec. 6.1.1.
[58] D. T. Cromer and J. B. Mann, J. Chem. Phys. **47**, 1892 (1967).
[59] D. T. Cromer, J. Chem. Phys. **50**, 4857 (1969).
[60] P. Chirawatkul (private communication).
[61] R. L. McGreevy and L. Pusztai, Proc. R. Soc. London, Ser. A **430**, 241 (1990).
[62] L. Pusztai and R. L. McGreevy, J. Non-Cryst. Solids **117-118**, 627 (1990).
[63] L. Pusztai and R. L. McGreevy, J. Phys.: Condens. Matter **13**, 7213 (2001).
[64] B. Brehler, Naturwiss. **46**, 554 (1959).
[65] H. R. Oswald and H. Jaggi, Helv. Chim. Acta **43**, 72 (1960).
[66] B. Brehler, Z. Kristallogr. **115**, 373 (1961).
[67] A. Zeidler, Ph.D. thesis, University of Bath, 2009.
[68] L. Hefeng, L. Kunquan, W. Zhonghua, and D. Jun, J. Phys.: Condens. Matter **6**, 3629 (1994).
[69] J. Wong and F. W. Little, J. Non-Cryst. Solids **37**, 273 (1980).
[70] K. Kadono, H. Kageyama, N. Kamijo, and H. Tanaka, J. Non-Cryst. Solids **140**, 98 (1992).
[71] C. Fillaux, B. Couzinet, C. Dreyfus, J. P. Itié, and A. Polian, Phys. Scr. **T115**, 339 (2005).
[72] B. van Laar and W. B. Yelon, J. Appl. Crystallogr. **17**, 47 (1984).
[73] L. W. Finger, D. E. Cox, and A. P. Jephcoat, J. Appl. Crystallogr. **27**, 892 (1994).
[74] P. S. Salmon, I. Petri, P. H. K. de Jong, P. Verkerk, H. E. Fischer, and W. S. Howells, J. Phys.: Condens. Matter **16**, 195 (2004).
[75] W. S. Howells, Nucl. Instrum. Methods Phys. Res. **219**, 543 (1984).
[76] M. G. Tucker, D. A. Keen, J. S. O. Evans, and M. T. Dove, J. Phys.: Condens. Matter **19**, 335215 (2007).
[77] S. Le Roux and P. Jund, Comput. Mater. Sci. **49**, 70 (2010).
[78] S. Le Roux and V. Petkov, J. Appl. Crystallogr. **43**, 181 (2010).
[79] R. Ruberto, G. Pastore, and M. P. Tosi, Physica B **405**, 974 (2010).
[80] G. D. Scott and D. M. Kilgour, J. Phys. D: Appl. Phys. **2**, 863 (1969).
[81] J. L. Finney, Proc. R. Soc. London, Ser. A **319**, 479 (1970).
[82] U. Müller, *Inorganic Structural Chemistry* (Wiley, Chichester, 1993).
[83] J. D. Bernal, I. A. Cherry, J. L. Finney, and K. R. Knight, J. Phys. E **3**, 388 (1970).
[84] C. Massobrio, A. Pasquarello, and R. Car, Phys. Rev. Lett. **80**, 2342 (1998).
[85] C. Massobrio, A. Pasquarello, and R. Car, J. Am. Chem. Soc. **121**, 2943 (1999).
[86] C. Massobrio, A. Pasquarello, and R. Car, Comput. Mater. Sci. **17**, 115 (2000).
[87] C. Massobrio, A. Pasquarello, and R. Car, Phys. Rev. B **64**, 144205 (2001).
[88] C. Massobrio and A. Pasquarello, Phys. Rev. B **68**, 020201(R) (2003).
[89] C. Massobrio, M. Celino, and A. Pasquarello, Phys. Rev. B **70**, 174202 (2004).
[90] C. Massobrio and A. Pasquarello, Phys. Rev. B **75**, 014206 (2007).
[91] M. Wilson and B. K. Sharma, J. Chem. Phys. **128**, 214507 (2008).
[92] M. Wilson, B. K. Sharma, and C. Massobrio, J. Chem. Phys. **128**, 244505 (2008).
[93] C. Massobrio and A. Pasquarello, Phys. Rev. B **77**, 144207 (2008).
[94] M. Micoulaut, R. Vuilleumier, and C. Massobrio, Phys. Rev. B **79**, 214205 (2009).
[95] C. Massobrio, Lect. Notes Phys. **795**, 343 (2010).
[96] C. Massobrio, M. Micoulaut, and P. S. Salmon, Solid State Sci. **12**, 199 (2010).
[97] M. Cobb, D. A. Drabold, and R. L. Cappelletti, Phys. Rev. B **54**, 12162 (1996).
[98] P. S. Salmon, J. Phys.: Condens. Matter **17**, S3537 (2005).
[99] P. S. Salmon, A. C. Barnes, R. A. Martin, and G. J. Cuello, Phys. Rev. Lett. **96**, 235502 (2006).
[100] P. S. Salmon, J. Phys.: Condens. Matter **18**, 11443 (2006).
[101] P. S. Salmon, A. C. Barnes, R. A. Martin, and G. J. Cuello, J. Phys.: Condens. Matter **19**, 415110 (2007).
[102] J. O'M. Bockris, A. Pilla, and J. L. Barton, Revue de Chimie, Academia de la Republique Populaire Roumaine **7**, 59 (1962).
[103] J. Zarzycki and F. Naudin, Acad. Sci., Paris, C. R. **256**, 1282 (1963).
[104] L. V. Woodcock, C. A. Angell, and P. Cheeseman, J. Chem. Phys. **65**, 1565 (1976).
[105] P. J. Gardner and D. M. Heyes, Physica B **131**, 227 (1985).
[106] P. Ballone, G. Pastore, J. S. Thakur, and M. P. Tosi, Physica B **142**, 294 (1986).
[107] P. N. Kumta, P. A. Deymier, and S. H. Risbud, Physica B **153**, 85 (1988).
[108] M. Wilson and P. A. Madden, Phys. Rev. Lett. **72**, 3033 (1994).
[109] M. C. Abramo and A. Consolo, Physica B **205**, 408 (1995).
[110] M. Wilson and P. A. Madden, Phys. Rev. Lett. **80**, 532 (1998).
[111] D. K. Belashchenko and O. I. Ostrovskii, Russ. J. Phys. Chem. **77**, 1111 (2003).
[112] S. Huang, F. Yoshida, and W. Wang, J. Mol. Liq. **115**, 81 (2004).
[113] W.-G. Seo, H. Matsuura, and F. Tsukihashi, Metall. Mater. Trans. B **37**, 239 (2006).